

Collapse of a self-gravitating Bose-Einstein condensate with attractive self-interaction

Pierre-Henri Chavanis

Laboratoire de Physique Théorique, Université Paul Sabatier, 118 route de Narbonne 31062 Toulouse, France

We study the collapse of a self-gravitating Bose-Einstein condensate with attractive self-interaction. Equilibrium states in which the gravitational attraction and the attraction due to the self-interaction are counterbalanced by the quantum pressure (Heisenberg uncertainty principle) exist only below a maximum mass $M_{\max} = 1.012\hbar/\sqrt{Gm|a_s|}$ where $a_s < 0$ is the scattering length of the bosons and m is their mass [Chavanis, Phys. Rev. D **84**, 043531 (2011)]. For $M > M_{\max}$ the system is expected to collapse and form a black hole. We study the collapse dynamics by making a Gaussian ansatz for the wave function and reducing the problem to the study of the motion of a particle in an effective potential. We find that the collapse time scales as $(M/M_{\max} - 1)^{-1/4}$ for $M \rightarrow M_{\max}^+$ and as $M^{-1/2}$ for $M \gg M_{\max}$. Other analytical results are given above and below the critical point corresponding to a saddle node bifurcation. We apply our results to standard axions with mass $m = 10^{-4} \text{ eV}/c^2$ and scattering length $a_s = -5.8 \times 10^{-53} \text{ m}$ for which $M_{\max} = 6.5 \times 10^{-14} M_{\odot}$ and $R = 3.3 \times 10^{-4} R_{\odot}$. We confirm our previous claim that bosons with attractive self-interaction, such as standard axions, may form low mass stars (axion stars or dark matter stars) but cannot form dark matter halos of relevant mass and size. These mini axions stars could be the constituents of dark matter. They can collapse into mini black holes of mass $\sim 10^{-14} M_{\odot}$ in a few hours. In that case, dark matter halos would be made of mini black holes. We also apply our results to ultralight axions with mass $m = 1.93 \times 10^{-20} \text{ eV}/c^2$ and scattering length $a_s = -8.29 \times 10^{-60} \text{ fm}$ for which $M_{\max} = 0.39 \times 10^6 M_{\odot}$ and $R = 33 \text{ pc}$. These ultralight axions could cluster into dark matter halos. Axionic dark matter halos with attractive self-interaction can collapse into supermassive black holes of mass $\sim 10^6 M_{\odot}$ (similar to those reported at the center of galaxies) in about one million years.

PACS numbers: 95.30.Sf, 95.35.+d, 98.80.-k

I. INTRODUCTION

The nature of dark matter is still unknown. It has been proposed that dark matter may be made of bosons in the form of Bose-Einstein condensates (BECs) at absolute zero temperature [1–65] (see [66–68] for reviews and the Introduction of [27] for a short historical account of the development of the BEC dark matter scenario). For dark matter halos, Newtonian gravity can be used so the evolution of the wave function of the self-gravitating BEC is governed by the Gross-Pitaevskii-Poisson (GPP) equations (see, e.g., [27–29]). By using the Madelung transformation [69], these equations can be written in the form of hydrodynamic equations, the so-called quantum Euler-Poisson (EP) equations. These equations are similar to the hydrodynamic equations of cold dark matter (CDM) except that they include a quantum force arising from the Heisenberg uncertainty principle and a pressure force due to the self-interaction of the bosons measured by their scattering length a_s . Quantum mechanics may be a way to solve the small scale problems of the CDM model such as the cusp problem, the missing satellite problem, and the “too big to fail” problem. In the BEC model, dark matter halos are stable equilibrium solutions of the GPP, or quantum EP, equations. They satisfy a condition of hydrostatic equilibrium corresponding to the balance between the quantum force (Heisenberg uncertainty principle), the pressure due to the self-interaction (scattering), and the gravitational attraction. The mass-radius relation of self-gravitating BECs at $T = 0$ has been

obtained numerically (exactly) and analytically (approximately) in [27, 28] for any value of the scattering length a_s of the bosons. This study makes the link between the noninteracting case $a_s = 0$ and the Thomas-Fermi (TF) limit $GM^2ma_s/\hbar^2 \gg 1$ in which the quantum potential can be neglected. It also treats the case of bosons with negative scattering lengths ($a_s < 0$).

When $a_s \geq 0$, the short-range interaction between the bosons is repulsive (or absent). In that case, there is a stable equilibrium state for any value of the mass M .¹ It corresponds to the balance between the repul-

¹ This is true in the Newtonian regime appropriate to dark matter halos. In the general relativistic regime, corresponding to boson stars (possibly mimicking massive black holes at the center of galaxies), equilibrium states exist only below a maximum mass. For noninteracting boson stars, the maximum mass is given by $M_{\max} = 0.633M_P^2/m$, where $M_P = (\hbar c/G)^{1/2} = 2.18 \times 10^{-8} \text{ kg}$ is the Planck mass. It is obtained from the Klein-Gordon-Einstein (KGE) equations [70, 71]. For self-interacting boson stars with a $\lambda\phi^4$ potential, the maximum mass is given by $M_{\max} = 0.0612\sqrt{\lambda}M_P^3/m^2$, where $\lambda = 8\pi a_s mc/\hbar$ is the dimensionless self-interaction constant (see Appendix A). It can be obtained from the KGE equations [72] or from their hydrodynamic representation [73]. In [73] it is argued that, because of their superfluid core, neutron stars could actually be BEC stars. Indeed, the neutrons could form Cooper pairs and behave as bosons of mass $2m_n$ (where $m_n = 0.940 \text{ GeV}/c^2$ is the mass of the neutron). By adjusting the value of the self-interaction constant, the maximum mass of these BEC stars could account for the abnormal mass (in the range $2 - 2.4 M_{\odot}$) of certain neutron stars [74–79] that is much larger than the Oppenheimer-Volkoff

sive quantum force, the repulsive self-interaction (if any), and the attractive gravitational force. When $a_s < 0$, the short-range interaction between the bosons is attractive. In that case, there is an equilibrium state only for $M \leq M_{\max}$ with [27, 28]:

$$M_{\max}^{\text{exact}} = 1.012 \frac{\hbar}{\sqrt{Gm|a_s|}}. \quad (1)$$

The stable configurations have a radius $R_{99} \geq R_{99}^*$ with [27, 28]:

$$(R_{99}^*)^{\text{exact}} = 5.5 \left(\frac{|a_s| \hbar^2}{Gm^3} \right)^{1/2}, \quad (2)$$

where the subscript 99 means that R_{99} is the radius containing 99% of the mass (the density profile has not a compact support but extends to infinity so the radius of the system is formally infinite). This equilibrium state corresponds to the balance between the repulsive quantum force, the attractive force coming from the self-interaction of the bosons, and the attractive gravitational force. For $M > M_{\max}$, there is no equilibrium state anymore because the quantum force cannot balance the attractive self-interaction and the gravitational attraction. In that case, nothing can prevent the collapse of the BEC, not even quantum mechanics (Heisenberg uncertainty principle). Therefore, the system is expected to collapse and form a black hole.

In the case of an attractive self-interaction, the maximum mass obtained in [27, 28] is usually extremely small. This is because it can be rewritten as [27]:²

$$M_{\max}^{\text{exact}} = 5.073 \frac{M_P}{\sqrt{|\lambda|}}. \quad (3)$$

Similarly, the maximum radius can be written as [27]:

$$(R_{99}^*)^{\text{exact}} = 1.1 \sqrt{|\lambda|} \frac{M_P}{m} \lambda_c, \quad (4)$$

where $\lambda_c = \hbar/mc$ is the Compton wavelength of the bosons. Unless the self-interaction constant λ is extraordinarily small, the maximum mass and the corresponding radius of self-gravitating BECs with attractive self-interaction are much smaller than the masses and radii of dark matter halos [27].

limit $M_{\text{OV}} = 0.376 M_P^3/m^2 = 0.7 M_\odot$ based on the assumption that neutron stars are ideal fermion stars [80].

² This scaling can be compared to the scaling $M_{\max} = 0.376 M_P^3/m^2$ of the maximum mass of fermion stars [80], to the scaling $M_{\max} = 0.633 M_P^2/m$ of the maximum mass of non-interacting boson stars [70, 71] and to the scaling $M_{\max} = 0.062 \sqrt{\lambda} M_P^3/m^2$ of the maximum mass of self-interacting boson stars [72, 73]. We emphasize, however, that the maximum mass given by Eq. (3) is a Newtonian result contrary to the other limits that come from general relativity. The usually very small value of the maximum mass (or mass-radius ratio) of self-gravitating BECs with attractive self-interaction justifies *a posteriori* why a Newtonian treatment is sufficient to describe them (see Appendix E for more details).

This remark has important consequences. It has often been proposed, in connection to the BEC dark matter model, that one possible dark matter candidate could be the axion [81, 82]. One reason is that, unlike the Higgs boson, axions are sufficiently long-lived to coalesce into dark matter halos which constitute the seeds of galaxy formation. Axions are hypothetical pseudo-Nambu-Goldstone bosons of the Peccei-Quinn phase transition associated with a $U(1)$ symmetry that solves the strong charge parity (CP) problem of quantum chromodynamics (QCD) [83]. Axions also appear in string theory leading to the notion of string axiverse [84]. The axion is a spin-0 particle with a very small mass and an extremely weak self-interaction arising from nonperturbative effects in QCD. Axions are extremely nonrelativistic and have huge occupation numbers, so they can be described by a classical field. Recently, it has been proposed that axionic dark matter can form a BEC during the radiation-dominated era [85, 86]. Axions can thus be described by a relativistic quantum field theory with a real scalar field ϕ whose evolution is governed by the Klein-Gordon-Einstein (KGE) equations. In the nonrelativistic limit, they can be described by an effective field theory with a complex scalar field ψ whose evolution is governed by the GPP equations. Therefore, axions seem to be good candidates for the BEC dark matter scenario. However, the axion has a negative scattering length corresponding to an attractive self-interaction. Therefore, according to the results of [27], it is not obvious that axions can form dark matter halos of relevant mass and size. This can be checked by a simple numerical application. Eqs. (1) and (2) can be rewritten as

$$\frac{M_{\max}^{\text{exact}}}{M_\odot} = 1.56 \times 10^{-34} \left(\frac{\text{eV}/c^2}{m} \right)^{1/2} \left(\frac{\text{fm}}{|a_s|} \right)^{1/2}, \quad (5)$$

$$\frac{(R_{99}^*)^{\text{exact}}}{R_\odot} = 1.36 \times 10^9 \left(\frac{|a_s|}{\text{fm}} \right)^{1/2} \left(\frac{\text{eV}/c^2}{m} \right)^{3/2}. \quad (6)$$

Considering standard axions with $m = 10^{-4} \text{eV}/c^2$ and $a_s = -5.8 \times 10^{-53} \text{m}$ [81], corresponding to $\lambda = -7.4 \times 10^{-49}$, we obtain $M_{\max}^{\text{exact}} = 6.5 \times 10^{-14} M_\odot$ and $(R_{99}^*)^{\text{exact}} = 3.3 \times 10^{-4} R_\odot$ (the average density is $\bar{\rho} = 2.55 \times 10^3 \text{g}/\text{m}^3$). These values are “ridiculously small” [27] as compared to the typical values of dark matter halos (they rather correspond to the typical size of asteroids). Obviously, standard axions cannot form dark matter halos of relevant mass and size.³ However, they could form mini boson stars (axion stars or dark matter stars) of very low mass which are stable gravitationally

³ The same conclusion can also be obtained by considering the gravitational instability of an infinite homogeneous distribution of BECs. This quantum Jeans problem has been studied in detail in [27, 34, 52] in the general case.

bound BECs. They might play a role as dark matter components (i.e. dark matter halos could be made of mini axion stars) if they exist in the universe in abundance. These mini axions stars could collapse into mini black holes of mass $\sim 10^{-14} M_\odot$. In that case, dark matter halos would be made of mini black holes (their evaporation time $t_e = 5120\pi G^2 M^3 / \hbar c^4 \sim 6.6 \times 10^{32}$ s is much larger than the age of the universe) and behave as CDM.

This conclusion only applies to the type of axions with attractive self-interaction that we have considered previously (“standard” axions). Axions with a repulsive self-interaction (if they exist) or axions with an attractive self-interaction, or no self-interaction, and an extraordinarily small mass could form bigger objects, possibly dark matter halos. To be specific, let us consider that the smallest dark matter halo that we know, Willman 1 ($R = 33$ pc, $M = 0.39 \times 10^6 M_\odot$, $\bar{\rho} = 1.75 \times 10^{-16}$ g/m³), is a pure BEC without atmosphere.⁴ Assuming that the bosons have a repulsive self-interaction and using the constraint $(|a_s|/\text{fm})^2 (\text{eV}/mc^2) \leq 1.77 \times 10^{-8}$ set by the Bullet Cluster, we obtain $m = 1.69 \times 10^{-2}$ eV/ c^2 , $a_s = 1.73 \times 10^{-5}$ fm and $\lambda = 3.72 \times 10^{-14}$ (see Appendix D of [87]). Assuming that the bosons have no self-interaction, we obtain $m = 2.57 \times 10^{-20}$ eV/ c^2 (see Appendix D of [87]). Finally, assuming that the bosons have an attractive self-interaction and using Eqs. (5) and (6), we obtain $m = 1.93 \times 10^{-20}$ eV/ c^2 , $a_s = -8.29 \times 10^{-60}$ fm and $\lambda = -2.04 \times 10^{-86}$. This is a new prediction (especially the scattering length). These values reproduce the mass and size of dwarf dark matter halos. On the other hand, the Bullet Cluster constraint is clearly satisfied. The values of m and a_s that we have obtained above may be revised by considering possibly more relevant dark matter halos than Willman 1 but their orders of magnitude should be correct. Therefore, it is not impossible that axions cluster into dark matter halos but, for that, their mass m and scattering length a_s need to have very different values from their “standard” values given previously. We shall call them “ultralight” axions. Axionic dark matter halos made of ultralight axions could collapse into supermassive black holes of mass $\sim 10^6 M_\odot$ similar to those reported at the center of galaxies.

In this paper, we study the collapse of a self-gravitating BEC with attractive self-interaction (e.g. an axion star or an axionic dark matter halo) when its mass is larger than the maximum mass obtained in [27]. To study this complex dynamics, we use in this paper a simple analytical model in which the collapse of the BEC is reduced

to the study of the motion of a particle in an effective potential $V(R)$, where R represents the size of the BEC. For $M > M_{\text{max}}$, the effective potential has no minimum so the particle descends the potential until the singular point of collapse at $R = 0$. This mechanical model, based on a Gaussian ansatz for the wave function, was introduced in the context of self-gravitating BECs in [27] (see [90] for generalizations). This type of approximation is standard in the study of BECs without self-gravity. It is known to give a good qualitative description of the evolution of the system but it is not always quantitatively accurate. Therefore, it would be important to carry in parallel a numerical study based on the KGE or GPP equations to compare our approximate analytical results to the exact numerical ones.

The paper is organized as follows. In Sec. II, we recall the GPP equations and their hydrodynamic representation. In Sec. III, we make a Gaussian ansatz for the wave function and recall the dynamical equation, obtained in [27, 90], satisfied by the radius $R(t)$ of the condensate. The stationary states of this equation provide an analytical expression of the mass-radius relation of self-gravitating BECs. We consider in this paper the case of a negative scattering length ($a_s < 0$) for which there is a maximum mass [27]. For $M < M_{\text{max}}$, two equilibrium states exist but only the configuration corresponding to the minimum of the effective potential is stable (this is the state with the largest radius). We calculate the radius, the energy and the complex pulsation as a function of the mass of the BEC and provide their asymptotic expressions in the nongravitational limit, the noninteracting limit, and close to the critical point. For $M \rightarrow M_{\text{max}}^-$, the period of the oscillations scales as $(1 - M/M_{\text{max}})^{-1/4}$. In Sec. IV, we study the collapse of the BEC for $M > M_{\text{max}}$ and determine the general expression of the collapse time as a function of the mass of the BEC in the form of an integral. In Sec. V, we show that the collapse time scales as $M^{-1/2}$ in the TF limit $M \gg M_{\text{max}}$. In Sec. VI, we study the collapse of the BEC close to the critical point $M \rightarrow M_{\text{max}}^+$ corresponding to a saddle node bifurcation. We find that the collapse time scales as $(M/M_{\text{max}} - 1)^{-1/4}$ for $M \rightarrow M_{\text{max}}^+$. In Secs. VII and VIII, we consider the possible collapse, explosion, or oscillations of the BEC when $M < M_{\text{max}}$. In Sec. IX, we conclude our study by applying our results to the case of axion stars and axionic dark matter halos. In Appendix A, we derive the GP equation from the KG equation in the nonrelativistic limit $c \rightarrow +\infty$ and connect the nonlinearity in the GP equation to the potential in the KG equation. In Appendix B, we discuss the Lagrangian structure of the GP equation in the scalar field and hydrodynamic representations and provide an alternative derivation of the effective mechanical model. In Appendix C, we show that the collapse of the BEC close to the critical point has a self-similar structure. In Appendix D, we highlight particular regimes of interest. In Appendix E, we study the validity of the Newtonian approximation used in our paper.

⁴ We assume that dwarf dark matter halos such as Willman 1 represent the ground state of a self-gravitating BEC (see Appendices D-F of [87]). Larger halos are more complex to study. They may be formed by hierarchical clustering. They have a core-halo structure in which the core is a pure BEC and the halo has a Navarro-Frenk-White (NFW) profile [88]. This core-halo structure may also result from a process of gravitational cooling [89]. In that case, the core is surrounded by a halo of scalar radiation.

II. THE GROSS-PITAEVSKII-POISSON EQUATIONS

We consider a self-gravitating BEC at $T = 0$ with short-range interactions. The evolution of the condensate wave function is governed by the GPP equations (see, e.g., [27–29]):

$$i\hbar\frac{\partial\psi}{\partial t} = -\frac{\hbar^2}{2m}\Delta\psi + m\Phi\psi + \frac{4\pi a_s\hbar^2}{m^2}|\psi|^2\psi, \quad (7)$$

$$\Delta\Phi = 4\pi G|\psi|^2. \quad (8)$$

The mass density of the bosons is $\rho = |\psi|^2$. The GP equation (7) can be seen as a nonlinear Schrödinger equation with a cubic nonlinearity. The self-interaction of the bosons is measured by their s -scattering length a_s which can be positive (repulsion) or negative (attraction).⁵

If we consider a wave function of the form $\psi = \sqrt{\rho(\mathbf{r})}e^{-iEt/\hbar}$, we obtain the time-independent GP equation

$$-\frac{\hbar^2}{2m}\Delta\psi + m\Phi\psi + \frac{4\pi a_s\hbar^2}{m^2}|\psi|^2\psi = E\psi. \quad (9)$$

Equations (8) and (9) form an eigenvalue problem for the wavefunction ψ , where E is the eigenvalue. We call it the eigenenergy.

By making the Madelung [69] transformation

$$\psi(\mathbf{r}, t) = \sqrt{\rho(\mathbf{r}, t)}e^{iS(\mathbf{r}, t)/\hbar}, \quad (10)$$

where

$$S = -i\frac{\hbar}{2}\ln\left(\frac{\psi}{\psi^*}\right) \quad (11)$$

is the action and

$$\mathbf{u}(\mathbf{r}, t) = \frac{\nabla S(\mathbf{r}, t)}{m} \quad (12)$$

is the (irrotational) velocity field, one finds that the GPP equations are equivalent to the hydrodynamic equations (see, e.g., [27–29]):

$$\frac{\partial\rho}{\partial t} + \nabla \cdot (\rho\mathbf{u}) = 0, \quad (13)$$

⁵ The GP equation (7) describes the evolution of the condensate wave function $\psi(\mathbf{r}, t)$ of a gas of bosons in interaction at $T = 0$. It is usually derived from the mean field Schrödinger equation [91, 92] when the short-range interaction between the bosons corresponds to binary collisions that can be modeled by a pair contact potential (see, e.g., Sec. II.A. of [27]). The GP equation can also be derived from the KG equation in the nonrelativistic limit $c \rightarrow +\infty$ (see Appendix A). In that case, the cubic nonlinearity in Eq. (7) corresponds to a quartic potential of the form $V(|\phi|) = (\lambda/4\hbar c)|\phi|^4$ in the KG equation. The self-interaction constant λ in the scalar field theory is related to the s -scattering length of the bosons by $\lambda = 8\pi a_s mc/\hbar$ [27].

$$\frac{\partial S}{\partial t} + \frac{1}{2m}(\nabla S)^2 + m\Phi + \frac{4\pi a_s\hbar^2}{m^2}\rho + Q = 0, \quad (14)$$

$$\frac{\partial\mathbf{u}}{\partial t} + (\mathbf{u} \cdot \nabla)\mathbf{u} = -\frac{1}{\rho}\nabla P - \nabla\Phi - \frac{1}{m}\nabla Q, \quad (15)$$

$$\Delta\Phi = 4\pi G\rho, \quad (16)$$

called the quantum EP equations. Equation (13) is the continuity equation, Eq. (14) is the quantum Hamilton-Jacobi (or Bernoulli) equation, and Eq. (15) is the quantum Euler equation. It involves the quantum potential

$$Q = -\frac{\hbar^2}{2m}\frac{\Delta\sqrt{\rho}}{\sqrt{\rho}} = -\frac{\hbar^2}{4m}\left[\frac{\Delta\rho}{\rho} - \frac{1}{2}\frac{(\nabla\rho)^2}{\rho^2}\right] \quad (17)$$

taking into account the Heisenberg uncertainty principle, and a pressure

$$P = \frac{2\pi a_s\hbar^2}{m^3}\rho^2 \quad (18)$$

taking into account the self-interaction of the bosons [93, 94]. The equation of state (18) is that of a polytrope of index $n = 1$ [95]. The stationary solution of the quantum Bernoulli equation (14), corresponding to $S = -Et$, writes

$$E = m\Phi + \frac{4\pi a_s\hbar^2}{m^2}\rho + Q. \quad (19)$$

This equation is equivalent to Eq. (9). The stationary solution of the quantum Euler equation (15) satisfies the condition of hydrostatic equilibrium

$$\nabla P + \rho\nabla\Phi + \frac{\rho}{m}\nabla Q = \mathbf{0}. \quad (20)$$

This is the gradient of Eq. (19). Combining Eq. (20) with the Poisson equation (8), we obtain the differential equation

$$-\frac{4\pi a_s\hbar^2}{m^3}\Delta\rho + \frac{\hbar^2}{2m^2}\Delta\left(\frac{\Delta\sqrt{\rho}}{\sqrt{\rho}}\right) = 4\pi G\rho. \quad (21)$$

This equation has been studied analytically and numerically in the general case (i.e. accounting for the quantum pressure and the self-interaction) in [27, 28]. The Jeans problem associated with the quantum EP equations (13)–(16) has been studied in [27] in a static background and in [34, 52] in an expanding background.

III. ANALYTICAL MODEL

A. The Gaussian ansatz

In general, the GPP equations (7) and (8) must be solved numerically. However, we can obtain approximate

analytical results by using a Gaussian ansatz for the wave function [27, 90]:

$$\psi(\mathbf{r}, t) = \left[\frac{M}{\pi^{3/2} R(t)^3} \right]^{1/2} e^{-\frac{r^2}{2R(t)^2}} e^{imH(t)r^2/2\hbar}, \quad (22)$$

where $R(t)$ measures the spatial extension of the system (wave packet). We shall call it the radius of the BEC. In the hydrodynamic representation, the density is given by

$$\rho(\mathbf{r}, t) = \frac{M}{[\pi R(t)^2]^{3/2}} e^{-\frac{r^2}{R(t)^2}}, \quad (23)$$

the action by

$$S(\mathbf{r}, t) = \frac{1}{2} m H(t) r^2, \quad (24)$$

and the velocity field by

$$\mathbf{u}(\mathbf{r}, t) = H(t)\mathbf{r}. \quad (25)$$

One can easily check [27, 90] that the continuity equation (13) is exactly satisfied by the ansatz (22) provided that

$$H(t) = \frac{\dot{R}}{R}. \quad (26)$$

This function is similar to the Hubble function in cosmology although the analogy is purely formal (see Sec. III C for a development of this analogy).

B. The gross dynamics

With the Gaussian ansatz, one can show (see [27, 90] and Appendix B) that the total energy of the BEC writes

$$E_{\text{tot}} = \frac{1}{2} \alpha M \left(\frac{dR}{dt} \right)^2 + V(R) \quad (27)$$

with

$$V(R) = \sigma \frac{\hbar^2 M}{m^2 R^2} + \zeta \frac{2\pi a_s \hbar^2 M^2}{m^3 R^3} - \nu \frac{GM^2}{R}, \quad (28)$$

where $\alpha = 3/2$, $\sigma = 3/4$, $\zeta = 1/(2\pi)^{3/2}$ and $\nu = 1/\sqrt{2\pi}$. The first term in Eq. (27) is the classical kinetic energy Θ_c and the second term in Eq. (27) is the potential energy. The potential energy contains the contribution of the quantum kinetic energy Θ_Q (or quantum potential), the internal energy U due to the self-interaction, and the gravitational energy W . It can be shown that the GPP and EP equations conserve the total energy E_{tot} and the mass M [27, 90]. Of course, these quantities must also be conserved by the gross dynamics resulting from the Gaussian ansatz. Writing $\dot{E}_{\text{tot}} = 0$, we find that the dynamical equation satisfied by the radius of the BEC is

$$\alpha M \frac{d^2 R}{dt^2} = -V'(R). \quad (29)$$

This equation is similar to the equation of motion of a particle of mass αM moving in an effective potential $V(R)$. This equation can also be obtained from the virial theorem satisfied by the GPP and EP equations [27, 90], or from the Euler-Lagrange equations (see Appendix B), when a trial wave function parametrized by a function of R , such as the one in Eq. (22), is introduced.

It can be shown from general arguments [96] that a stable equilibrium state of the GPP and EP equations is a minimum of the total energy E_{tot} at fixed mass M [27]. This is also true for the gross dynamics: a stable equilibrium state of Eq. (29) is a minimum of the total energy $E_{\text{tot}}(R, \dot{R})$ at fixed mass M . A necessary condition for equilibrium is that $\dot{R} = 0$ meaning that the radius of the BEC is stationary. Then, the equilibrium radius R of the BEC, when an equilibrium state exists, is a minimum of the effective potential $V(R)$. The condition $V'(R) = 0$ leads to the general analytical mass-radius relation of a self-gravitating BEC with short-range interactions [27]:

$$M = \frac{2\sigma}{\nu} \frac{\frac{\hbar^2}{Gm^2 R}}{1 - \frac{6\pi\zeta a_s \hbar^2}{\nu G m^3 R^2}}. \quad (30)$$

For $M \rightarrow 0$ and $R \rightarrow +\infty$, we recover the relation

$$R \sim \frac{2\sigma}{\nu} \frac{\hbar^2}{GMm^2} \quad (31)$$

corresponding to a noninteracting self-gravitating BEC ($a_s = 0$) [27]. The radius R_{99} containing 99% of the mass is $R_{99} = 8.955\hbar^2/GMm^2$. It is in good agreement with the exact result $R_{99} = 9.9\hbar^2/GMm^2$ [3, 28, 71].

C. Analogy with cosmology

The first integral of motion given by Eqs. (27) and (28) can be rewritten as

$$\left(\frac{\dot{R}}{R} \right)^2 = \frac{2E_{\text{tot}}}{\alpha MR^2} + \frac{2\nu GM}{\alpha R^3} - \frac{2\sigma\hbar^2}{\alpha m^2 R^4} - \frac{4\pi\zeta a_s \hbar^2 M}{\alpha m^3 R^5}. \quad (32)$$

In the case where the quantum potential and the self-interaction can be neglected, it reduces to

$$\left(\frac{\dot{R}}{R} \right)^2 = \frac{2E_{\text{tot}}}{\alpha MR^2} + \frac{2\nu GM}{\alpha R^3}. \quad (33)$$

This is similar to the Friedmann equation in cosmology

$$H^2 = \left(\frac{\dot{R}}{R} \right)^2 = -\frac{kc^2}{R^2} + \frac{8\pi G}{3c^2} \epsilon \quad (34)$$

for a pressureless ($P = 0$) universe whose energy density decreases as $\epsilon \propto R^{-3}$ [97] (see the Introduction of

[98] for a short historic of the early development of cosmology). In this analogy R plays the role of the scale factor, $H = \dot{R}/R$ plays the role of the Hubble parameter, $-2E_{\text{tot}}/\alpha M$ plays the role of the curvature constant kc^2 , and $2\nu M/\alpha R^3$ plays the role of the mass density $8\pi\epsilon/3c^2$ with $\epsilon/c^2 \propto R^{-3}$. We can therefore draw certain analogies between the evolution of a self-gravitating BEC and the evolution of a Friedmann-Lemaître-Robertson-Walker (FLRW) universe.

Remark: In a universe filled with a fluid with an equation of state $P = \alpha\epsilon$, the energy density is related to the scale factor by $\epsilon \propto R^{-3(1+\alpha)}$. If we take into account all the terms in Eq. (32), we find that the quantum potential term is analogous to an energy density $\epsilon \propto -1/R^4$ in cosmology. This corresponds to $\alpha = 1/3$ like for the standard radiation. However, the energy density is negative. On the other hand, the self-interaction term is analogous to an energy density $\epsilon \propto \mp/R^5$ in cosmology. This corresponds to $\alpha = 2/3$ (to our knowledge, this coefficient has not been considered in cosmology). The energy density is negative when $a_s > 0$ and a positive when $a_s < 0$.

D. BECs with negative scattering length

In this paper, we focus on the case of an attractive self-interaction corresponding to a negative scattering length ($a_s < 0$). In that case, there exists a maximum mass [27]:

$$M_{\text{max}} = \left(\frac{\sigma^2}{6\pi\zeta\nu} \right)^{1/2} \frac{\hbar}{\sqrt{Gm|a_s|}} \quad (35)$$

corresponding to a radius [27]:

$$R_* = \left(\frac{6\pi\zeta|a_s|\hbar^2}{\nu Gm^3} \right)^{1/2}. \quad (36)$$

Stable equilibrium states exist only for $M < M_{\text{max}}$. They have a radius $R > R_*$. We note that the approximate values of $M_{\text{max}} = 1.085\hbar/\sqrt{Gm|a_s|}$ and $R_{99}^* = 4.125(|a_s|\hbar^2/Gm^3)^{1/2}$ obtained within the Gaussian ansatz [27] are relatively close to the exact values $M_{\text{max}}^{\text{exact}} = 1.012\hbar/\sqrt{Gm|a_s|}$ and $(R_{99}^*)^{\text{exact}} = 5.5(|a_s|\hbar^2/Gm^3)^{1/2}$ obtained numerically by solving the GPP equations [28]. We note that the maximum mass M_{max} and the minimum stable radius R_* are related to each other by

$$M_{\text{max}} = \frac{\sigma}{\nu} \frac{\hbar^2}{Gm^2 R_*}. \quad (37)$$

It is convenient to introduce the energy scale

$$V_0 = \frac{\sigma^2\nu^{1/2}}{(6\pi\zeta)^{3/2}} \frac{\hbar m^{1/2} G^{1/2}}{|a_s|^{3/2}}. \quad (38)$$

Using Eqs. (35) and (36), we can check that V_0 is of the order of magnitude of $\hbar^2 M_{\text{max}}/m^2 R_*$, $|a_s|\hbar^2 M_{\text{max}}^2/m^3 R_*^3$

and GM_{max}^2/R_* . We also introduce the dynamical time

$$t_D = \left(\frac{\alpha M_{\text{max}} R_*^2}{V_0} \right)^{1/2} = \frac{6\pi\zeta}{\nu} \left(\frac{\alpha}{\sigma} \right)^{1/2} \frac{|a_s|\hbar}{Gm^2}. \quad (39)$$

Using Eqs. (35) and (36), we can check that t_D is of the order of magnitude of $(R_*^3/GM_{\text{max}})^{1/2} \sim 1/\sqrt{G\rho_{\text{max}}}$ where $\rho_{\text{max}} = 3M_{\text{max}}/4\pi R_*^3$ is a characteristic density equal to the maximum averaged density of the BEC. For standard axions with $m = 10^{-4}$ eV/ c^2 and $a_s = -5.8 \cdot 10^{-53}$ m, we obtain $M_{\text{max}} = 6.9 \times 10^{-14} M_\odot$, $R_* = 1.0 \times 10^{-4} R_\odot$, $V_0 = 7.1 \times 10^{21}$ g m²/s², $\rho_{\text{max}} = 9.73 \times 10^4$ g/m³, and $t_D = 1.2 \times 10^4$ s = 3.4 hrs. For ultralight axions with $m = 1.93 \times 10^{-20}$ eV/ c^2 and $a_s = -8.29 \times 10^{-60}$ fm, we obtain $M_{\text{max}} = 4.18 \times 10^5 M_\odot$, $R_* = 10.4$ pc, $V_0 = 5.74 \times 10^{46}$ g m²/s², $\rho_{\text{max}} = 6.00 \times 10^{-15}$ g/m³, and $t_D = 4.70 \times 10^{13}$ s = 1.49 Myrs.

E. The dynamical equation

We introduce the dimensionless variables

$$\hat{M} = \frac{M}{M_{\text{max}}}, \quad \hat{R} = \frac{R}{R_*}, \quad \hat{V} = \frac{V}{V_0}, \quad (40)$$

$$\hat{t} = \frac{t}{t_D}, \quad \hat{\omega} = \omega t_D. \quad (41)$$

We shall work with these dimensionless variables but, from now on, we forget the ‘‘hats’’ in order to simplify the notations. The equation of motion (29) becomes

$$M \frac{d^2 R}{dt^2} = -V'(R) \quad (42)$$

with the effective potential

$$V(R) = \frac{M}{R^2} - \frac{M^2}{3R^3} - \frac{M^2}{R}. \quad (43)$$

The effective potential is plotted in Fig. 1. Equation (42) has the first integral

$$E_{\text{tot}} = \frac{1}{2} M \left(\frac{dR}{dt} \right)^2 + V(R), \quad (44)$$

where E_{tot} is a constant representing the total energy of the system. Equation (44) can be rewritten as

$$\frac{dR}{dt} = \pm \sqrt{\frac{2}{M} [E_{\text{tot}} - V(R)]}, \quad (45)$$

where the sign + corresponds to an expansion of the BEC ($\dot{R} > 0$) and the sign - to a contraction ($\dot{R} < 0$). Integrating Eq. (45) between 0 and t , we find that the evolution of the radius $R(t)$ of the BEC is determined by the equation

$$\int_{R_0}^{R(t)} \frac{dR}{\sqrt{E_{\text{tot}} - V(R)}} = \pm \left(\frac{2}{M} \right)^{1/2} t. \quad (46)$$

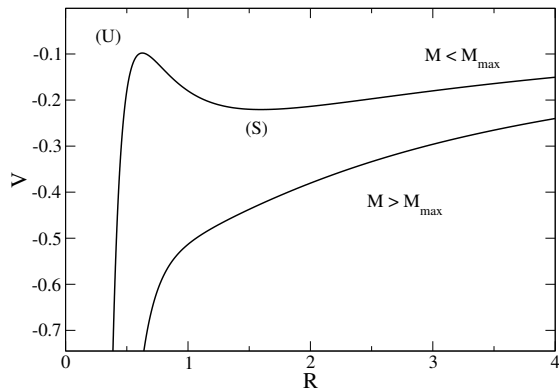


FIG. 1: Effective potential $V(R)$ as a function of the radius R for different values of the mass M . For illustration, we have taken $M = 0.9 < M_{\max}$ and $M = 1.1 > M_{\max}$ where $M_{\max} = 1$.

F. The mass-radius relation

A stable equilibrium state corresponds to a minimum of the effective potential $V(R)$. The condition $V'(R_e) = 0$ leads to the mass-radius relation

$$M = \frac{2R_e}{1 + R_e^2}, \quad (47)$$

or

$$R_e = \frac{1 \pm \sqrt{1 - M^2}}{M}. \quad (48)$$

The mass-radius relation is plotted in Fig. 2. Equilibrium states exist only below a maximum mass which is obtained from the condition $M'(R_e) = 0$ yielding $R_* = 1$ and $M_{\max} = 1$. For $M < M_{\max}$, there are two branches determining two possible radii $R_U(M) < 1$ and $R_S(M) > 1$ for the same mass M . However, a stable equilibrium state must be a *minimum* of $V(R)$ so it must satisfy $V''(R_e) > 0$. Computing the second derivative of $V(R)$ from Eq. (43) and using the mass-radius relation (47), we get

$$V''(R_e) = \frac{4(R_e^2 - 1)}{R_e^3(1 + R_e^2)^2}. \quad (49)$$

From this expression, we see that the branch (S) corresponding to $R_e > R_*$ is stable while the branch (U) corresponding to $R_e < R_*$ is unstable. Therefore, $R_* = 1$ represents the minimum possible radius of stable equilibrium states. The change of stability in the series of equilibria corresponds to the maximum mass M_{\max} in agreement with the Poincaré theorem and with the theory of catastrophes (see Sec. IIII).

For $M \rightarrow 0$ and $R_e \rightarrow 0$, we get $M \sim 2R_e$ and $V''(R_e) \sim -4/R_e^3$. In this limit, self-gravity is negligible so the equilibrium is due to the balance between

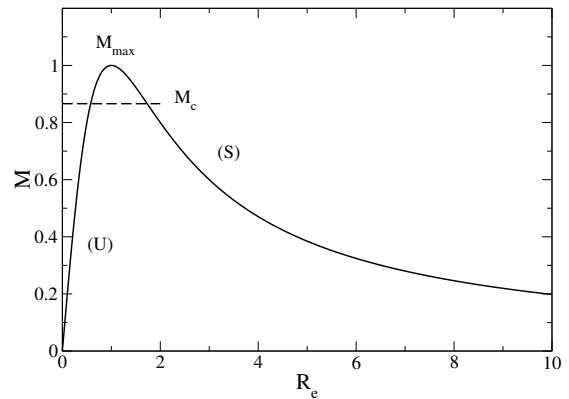


FIG. 2: Mass-radius relation of a self-gravitating BEC with attractive self-interaction. The mass M_c is defined in Sec. VII.

the repulsive quantum pressure and the attractive self-interaction (nongravitational limit). However, this equilibrium is unstable.

For $M \rightarrow 0$ and $R_e \rightarrow +\infty$, we get $M \sim 2/R_e$ and $V''(R_e) \sim 4/R_e^5$. In this limit, the self-interaction is negligible so the equilibrium is due to the balance between the repulsive quantum pressure and the attractive self-gravity (noninteracting limit). This equilibrium is stable. It corresponds to Newtonian noninteracting BEC stars.

For $M \rightarrow M_{\max}$ and $R \rightarrow R_*$, we get

$$M \simeq 1 - \frac{1}{2}(R_e - 1)^2, \quad R_e \simeq 1 \pm \sqrt{2(1 - M)}, \quad (50)$$

$$V''(R_e) \sim 2(R_e - 1). \quad (51)$$

These equations describe a saddle-node bifurcation where two equilibria (one stable and one unstable) merge and suddenly disappear at the critical point. For future purposes, it will be necessary to go to next order in the expansion of the mass-radius relation close to the critical point. We find

$$M \simeq 1 - \frac{1}{2}(R_e - 1)^2 + \frac{1}{2}(R_e - 1)^3, \quad (52)$$

$$R_e - 1 = \pm \sqrt{2(1 - M)} \left[1 \pm \frac{1}{2} \sqrt{2(1 - M)} \right]. \quad (53)$$

G. The total energy

At equilibrium, the total energy of a BEC with a mass M is given by $E_{\text{tot}} = V(R_e)$. Therefore

$$E_{\text{tot}} = \frac{M}{R_e^2} - \frac{M^2}{3R_e^3} - \frac{M^2}{R_e}. \quad (54)$$

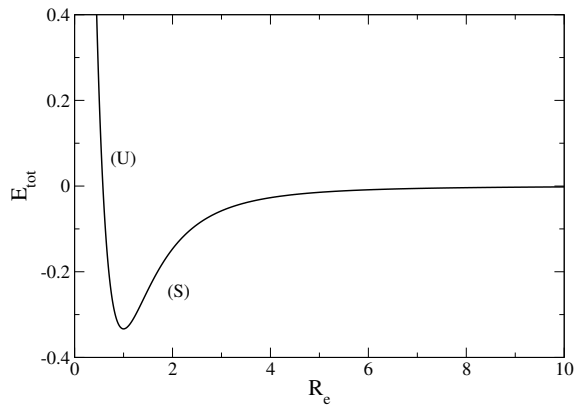


FIG. 3: Total energy as a function of the radius.

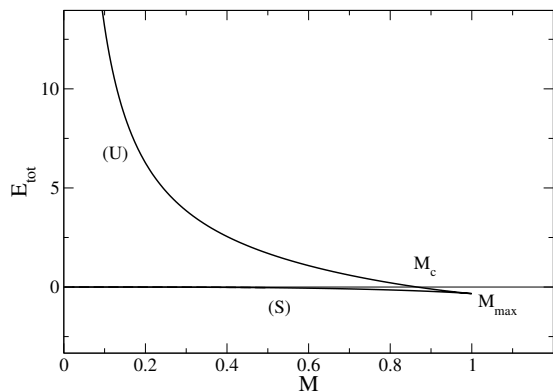


FIG. 4: Total energy as a function of the mass. The mass M_c is defined in Sec. VII.

We can obtain $E_{\text{tot}}(R_e)$ by using Eq. (47) to express M as a function of R_e . This gives

$$E_{\text{tot}} = \frac{2(1 - 3R_e^2)}{3R_e(1 + R_e^2)^2}. \quad (55)$$

This function is plotted in Fig. 3. We note that the minimum energy $E_{\text{tot}}^{\text{min}} = -1/3$ is reached for $R_e = R_* = 1$. Therefore, the change of stability in the series of equilibria corresponds to the minimum energy $E_{\text{tot}}^{\text{min}}$. We can obtain $E_{\text{tot}}(M)$ by using Eq. (48) to express R_e in terms of M . Alternatively, the function $E_{\text{tot}}(M)$ is given in parametric form by Eqs. (47) and (55) where the parameter is R_e . This function is plotted in Fig. 4. We can check that the stable branch (S) has a lower energy than the unstable branch as it should. We also recall that a necessary (but not sufficient) condition of nonlinear dynamical stability is that $E_{\text{tot}} < 0$. We can check that the stable branch satisfies this condition.

For $M \rightarrow 0$ and $R_e \rightarrow 0$ (nongravitational limit), we get $E_{\text{tot}}(R_e) \sim 2/3R_e$ and $E_{\text{tot}}(M) \sim 4/3M$.

For $M \rightarrow 0$ and $R_e \rightarrow +\infty$ (noninteracting limit), we get $E_{\text{tot}}(R_e) \sim -2/R_e^3$ and $E_{\text{tot}}(M) \sim -M^3/4$.

For $M \rightarrow M_{\text{max}}$ and $R \rightarrow R_*$ (critical point), we get

$$E_{\text{tot}}(R_e) \simeq -\frac{1}{3} + \frac{5}{6}(R_e - 1)^2 - \frac{3}{2}(R_e - 1)^3, \quad (56)$$

$$E_{\text{tot}}(M) \simeq -\frac{1}{3} + \frac{5}{3}(1 - M) \mp \frac{4}{3}\sqrt{2}(1 - M)^{3/2}, \quad (57)$$

where we used Eq. (53).

Since the functions $M(R_e)$ and $E_{\text{tot}}(R_e)$ achieve their extrema at the same point $M = R_* = 1$,⁶ the function $E_{\text{tot}}(M)$ presents a *spike* at the critical point $M = M_{\text{max}}$ (see Fig. 4).

H. The pulsation

We can analyze the stability of an equilibrium state by considering a small perturbation about equilibrium. We assume $M < M_{\text{max}}$ and write $R(t) = R_e + \epsilon(t)$ with $\epsilon(t) \ll 1$. Substituting this decomposition into Eq. (42) and keeping only terms that are linear in ϵ , we obtain

$$\frac{d^2\epsilon}{dt^2} + \omega^2\epsilon = 0, \quad (58)$$

where

$$\omega^2 = \frac{V''(R_e)}{M} \quad (59)$$

is the square of the complex pulsation. Clearly $\omega^2 > 0$ corresponds to a stable state which, when displaced from equilibrium, oscillates about equilibrium with a pulsation ω . By contrast, $\omega^2 < 0$ corresponds to an unstable state which, when displaced from equilibrium, evolves away from equilibrium with a growth rate $\gamma = \sqrt{-\omega^2}$. From these expressions, we confirm that a minimum of $V(R)$ is stable and a maximum of $V(R)$ is unstable. Furthermore, using Eqs. (47) and (49), we can express ω^2 as a function of the radius according to

$$\omega^2 = \frac{2(R_e^2 - 1)}{R_e^4(R_e^2 + 1)}. \quad (60)$$

This function is plotted in Fig. 5. The pulsation vanishes ($\omega^2 = 0$) at the critical point $M = M_{\text{max}} = 1$ and $R_e = R_* = 1$. The states with $R_e > 1$ are stable ($\omega^2 > 0$) and the states with $R_e < 1$ are unstable ($\omega^2 < 0$) in agreement with our previous discussion. We note that the maximum pulsation $(\omega^2)_{\text{max}} =$

⁶ The intrinsic reason is the following. A stable steady state of the GPP and EP equations is a minimum of E_{tot} at fixed mass M [27]. Introducing a Lagrange multiplier μ/m to take into account the mass constraint, the cancellation of the first order variations writes $\delta E_{\text{tot}} - (\mu/m)\delta M = 0$. This is valid for any equilibrium state in the series of equilibria. From that relation, $\delta M = 0$ implies $\delta E_{\text{tot}} = 0$. Therefore, the mass and the total energy achieve their extrema at the same point in the series of equilibria.

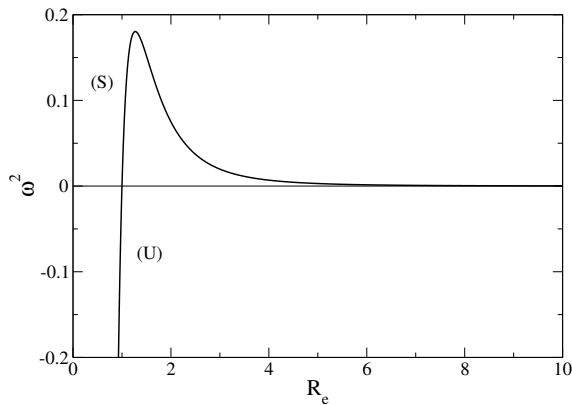


FIG. 5: Complex pulsation as a function of the radius.

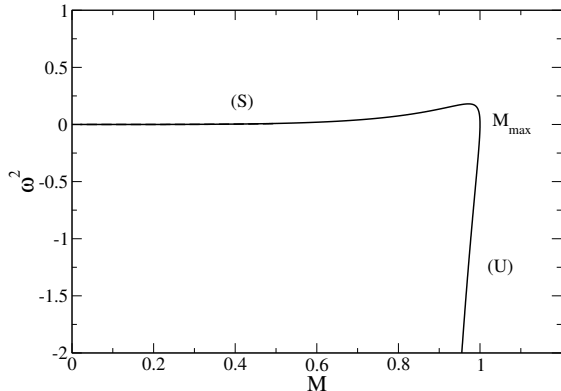


FIG. 6: Complex pulsation as a function of the mass.

$8(\sqrt{5} - 1)/[(\sqrt{5} + 3)(1 + \sqrt{5})^2] = 0.1803\dots$ is reached for $R_e = [(1 + \sqrt{5})/2]^{1/2} = 1.272\dots$ and $M = [8(1 + \sqrt{5})]^{1/2}/(3 + \sqrt{5}) = 0.9717\dots$. The function $\omega^2(M)$ is obtained in parametric form from Eqs. (47) and (60) where the parameter is R_e . This function is plotted in Fig. 6.

For $M \rightarrow 0$ and $R_e \rightarrow 0$ (nongravitational limit), we get $\omega^2 \sim -2/R_e^4$ and $\omega^2 \sim -32/M^4$.

For $M \rightarrow 0$ and $R_e \rightarrow +\infty$ (noninteracting limit), we get $\omega^2 \sim 2/R_e^4$ and $\omega^2 \sim M^4/8$.

For $M \rightarrow M_{\max}$ and $R_e \rightarrow R_*$ (critical point), we get

$$\omega^2 \sim 2(R_e - 1) \sim \pm 2\sqrt{2(1 - M)}. \quad (61)$$

I. The Poincaré theorem

According to Eqs. (47), (49) and (60), we have the relation

$$\frac{dM}{dR_e} = -\frac{1}{2}R_e^3V''(R_e) = -\frac{1}{2}MR_e^3\omega^2. \quad (62)$$

Close to the critical point, Eq. (62) reduces to

$$\frac{dM}{dR_e} = -\frac{1}{2}V''(R_e) = -\frac{\omega^2}{2} \quad (63)$$

which can be directly obtained from Eqs. (50), (51) and (61). These relations first show that the change of stability ($\omega^2 = 0$) corresponds to the turning point of mass ($M'(R_e) = 0$). Furthermore, they relate the stability of the system to the slope of the mass-radius relation $M(R_e)$. The branch where the mass increases with the radius ($M'(R_e) > 0$) is unstable ($\omega^2 < 0$) and the branch where the mass decreases with the radius ($M'(R_e) < 0$) is stable ($\omega^2 > 0$). These results are particular cases of the Poincaré theorem on the series of equilibria [99] (see [100, 101] for some applications of the Poincaré theorem to self-gravitating systems). They have been formalized in the theory of catastrophes.

IV. COLLAPSE OF THE BEC WHEN $M \geq M_{\max}$

We consider a BEC with a mass $M \geq M_{\max} = 1$ so that no equilibrium state exists. In that case, the BEC is expected to collapse and form a black hole. Here, we study the collapse analytically by using the gross dynamics defined by Eqs. (42) and (43).

A. The collapse time

To be specific, we consider an initial condition such that $\dot{R}_0 = 0$ (no initial velocity) although more general initial conditions could be considered as well. For this initial condition the total energy is $E_{\text{tot}} = V(R_0)$, where R_0 is the initial radius of the BEC. In that case, according to Eq. (46), the evolution of the radius $R(t)$ of the BEC is given by

$$\int_{R(t)}^{R_0} \frac{dR}{\sqrt{V(R_0) - V(R)}} = \left(\frac{2}{M}\right)^{1/2} t, \quad (64)$$

where the sign has been chosen so that $R(t)$ decreases with time since we are considering a collapse solution. The collapse time, corresponding to $R(t_{\text{coll}}) = 0$, is given by

$$t_{\text{coll}} = \left(\frac{M}{2}\right)^{1/2} \int_0^{R_0} \frac{dR}{\sqrt{V(R_0) - V(R)}}. \quad (65)$$

Using Eq. (65), we can rewrite Eq. (64) in the form

$$\int_0^{R(t)} \frac{dR}{\sqrt{V(R_0) - V(R)}} = \left(\frac{2}{M}\right)^{1/2} (t_{\text{coll}} - t). \quad (66)$$

For the potential of Eq. (43) the collapse time is given by

$$t_{\text{coll}} = \sqrt{\frac{M}{2}} \int_0^{R_0} \frac{dR}{\sqrt{\frac{M}{R_0^2} - \frac{M^2}{3R_0^3} - \frac{M^2}{R_0} - \frac{M}{R^2} + \frac{M^2}{3R^3} + \frac{M^2}{R}}}. \quad (67)$$

This is a function $t_{\text{coll}}(M, R_0)$ of the mass M of the BEC and of its initial radius R_0 .

The function $R_0 \mapsto t_{\text{coll}}(M, R_0)$ is plotted in Figs. 7, 8, 9 and 10 for different values of the mass M . The asymptotic behaviors of $R_0 \mapsto t_{\text{coll}}(M, R_0)$ for $R_0 \rightarrow 0$ and $R_0 \rightarrow +\infty$ are given by Eqs. (77) and (81). When $M = 1$, the collapse time $t_{\text{coll}}(M = 1, R_0)$ diverges when $R_0 \rightarrow 1$ according to Eqs. (106) and (109). For $M \rightarrow 1^+$ and $R_0 \rightarrow 1$, the function $R_0 \mapsto t_{\text{coll}}(M, R_0)$ has a self-similar structure discussed in Appendix C 3 and illustrated in Figs. 31 and 32. For $1 \leq M \leq M_* \simeq 1.0116$, the function $R_0 \mapsto t_{\text{coll}}(R_0, M)$ presents a local maximum at $((R_0)_M, (t_{\text{coll}})_M)$ and a local minimum at $((R_0)_m, (t_{\text{coll}})_m)$ as illustrated in Fig. 10. These characteristic values are plotted as a function of M in Figs. 11 and 12. For $M = 1$, we find $((R_0)_M, (t_{\text{coll}})_M) = (1, +\infty)$ and $((R_0)_m, (t_{\text{coll}})_m) = (1.67\dots, 7.0857\dots)$. For $M = M_*$, we find $((R_0)_M, (t_{\text{coll}})_M) = ((R_0)_m, (t_{\text{coll}})_m) = (1.31\dots, 6.257\dots)$.

The function $M \mapsto t_{\text{coll}}(M, R_0)$ is plotted in Figs. 13 and 14 for different values of the initial radius R_0 . The asymptotic behavior of $M \mapsto t_{\text{coll}}(M, R_0)$ for $M \rightarrow +\infty$ is given by Eq. (89). The value of $t_{\text{coll}}(M, R_0)$ at $M = 1$ is plotted as a function of R_0 in Figs. 8, 9 and 10 (as we have already mentioned, the function $R_0 \mapsto t_{\text{coll}}(R_0, M = 1)$ is non monotonic). When $R_0 = 1$, the collapse time $t_{\text{coll}}(M, R_0 = 1)$ diverges when $M \rightarrow 1^+$ according to Eqs. (112). For $M \rightarrow 1^+$ and $R_0 \rightarrow 1$, the function $M \mapsto t_{\text{coll}}(M, R_0)$ has a self-similar structure as shown in Appendixes C 1 and C 2 and illustrated in Fig. 28.

The evolution of the radius $R(t)$ of the BEC is represented in Fig. 15 for $M = 2$ and $R_0 = 1$ and in Fig. 16 for different values of M . The asymptotic behaviors of $R(t)$ for $t \rightarrow 0$ and $t \rightarrow t_{\text{coll}}$ are given by Eqs. (70) and (73). The universal self-similar evolution of the scaled radius close to the critical point $(M, R) = (1, 1)$ is given by Eqs. (C2), (C12) and (C23) and illustrated in Figs. 29, 30, and 33.

B. Behavior of $R(t)$ for $t \rightarrow 0$

For $t \rightarrow 0$, corresponding to $R \rightarrow R_0$, we can make the approximation $V(R) \simeq V(R_0) + V'(R_0)(R - R_0)$ with $V'(R_0) > 0$. Equation (64) becomes

$$\int_{R(t)}^{R_0} \frac{dR}{\sqrt{V'(R_0)(R_0 - R)}} = \left(\frac{2}{M}\right)^{1/2} t, \quad (68)$$

leading to

$$R(t) \simeq R_0 - \frac{1}{2M} V'(R_0) t^2. \quad (69)$$

For the potential of Eq. (43), Eq. (69) takes the form

$$R(t) \simeq R_0 - \frac{1}{2} \left[-\frac{2}{R_0^3} + \frac{M}{R_0^4} + \frac{M}{R_0^2} \right] t^2. \quad (70)$$

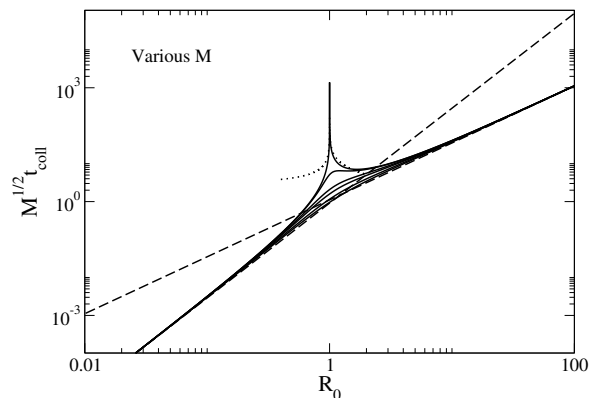


FIG. 7: Collapse time of the self-gravitating BEC as a function of its initial radius R_0 for different masses $M = 1, 1.01, 1.1, 1.2, 1.5, 2$ (top to bottom). For $M = 1$, the collapse time diverges when $R_0 \rightarrow 1$ (dotted lines) as detailed in Figs. 8 and 9. We note that the asymptotic behaviors of $\sqrt{M}t_{\text{coll}}(M, R_0)$ for $R_0 \rightarrow 0$ and $R_0 \rightarrow +\infty$ are independent of M (dashed lines). Furthermore, for $M \rightarrow +\infty$, the function $R_0 \mapsto M^{1/2}t_{\text{coll}}(M, R_0)$ tends to the function $A(R_0)$ defined by Eq. (90) and plotted in Fig. 17.

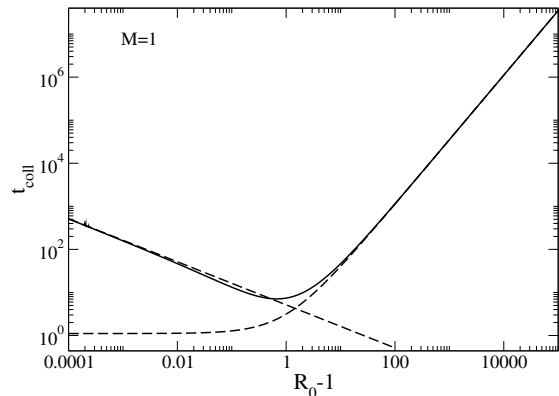


FIG. 8: Collapse time of the self-gravitating BEC as a function of its initial radius $R_0 \geq 1$ for $M = 1$.

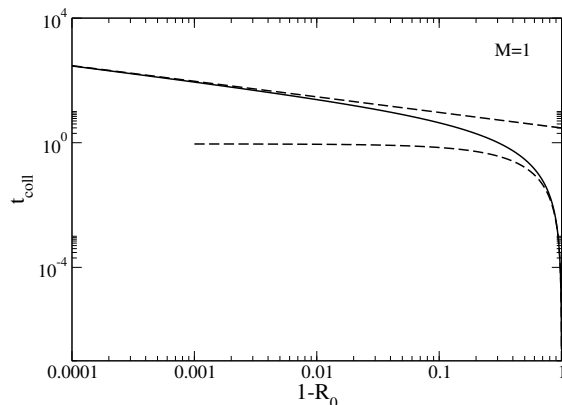


FIG. 9: Collapse time of the self-gravitating BEC as a function of its initial radius $R_0 \leq 1$ for $M = 1$.

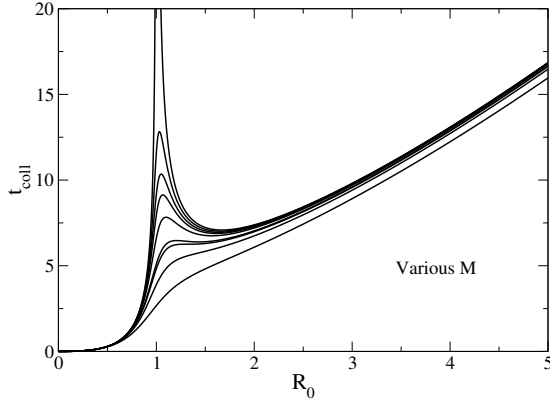


FIG. 10: Collapse time of the self-gravitating BEC as a function of its initial radius R_0 for different masses $M = 1, 1.001, 1.002, 1.003, 1.005, 1.01, 1.0116, 1.02, 1.05$ (top to bottom). For $1 \leq M \leq M_* = 1.0116$, the collapse time presents a local maximum at $((R_0)_M, (t_{\text{coll}})_M)$ and a local minimum at $((R_0)_m, (t_{\text{coll}})_m)$.

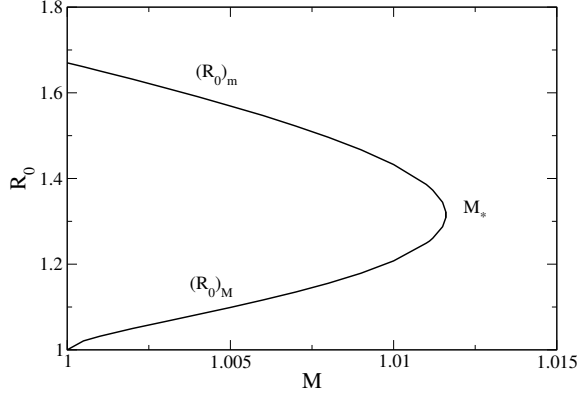


FIG. 11: Evolution of $(R_0)_M$ and $(R_0)_m$ as a function of M .

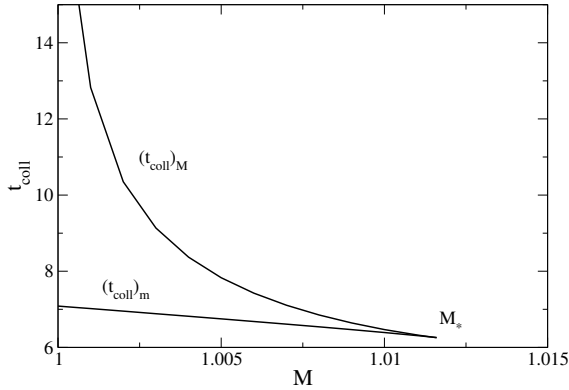


FIG. 12: Evolution of $(t_{\text{coll}})_M$ and $(t_{\text{coll}})_m$ as a function of M .

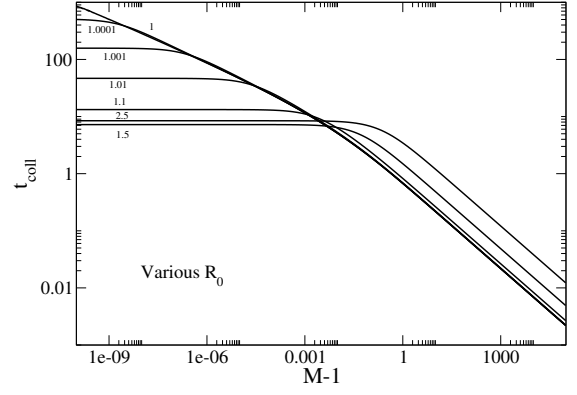


FIG. 13: Collapse time of the self-gravitating BEC as a function of its mass M for different values of the initial radius $R_0 = 1, 1.0001, 1.001, 1.01, 1.1, 1.5, 2.5$ (for clarity, we have restricted ourselves to $R_0 > 1$). For $R_0 = 1$, the collapse time diverges when $M \rightarrow 1^+$ as detailed in Fig. 14. We note that the evolution of $t_{\text{coll}}(M = 1, R_0)$ is non monotonic for $R_0 \geq 1$ in agreement with the results of Fig. 8. The plateau corresponding to $M \rightarrow 1$ first decreases as R_0 increases from $R_0 = 1$ to $(R_0)_m = 1.67\dots$, then increases as R_0 passes above $(R_0)_m = 1.67\dots$

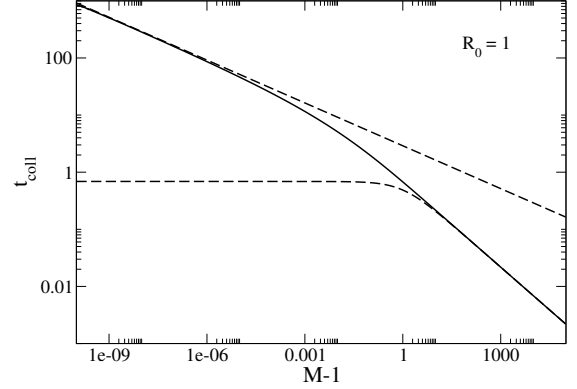


FIG. 14: Collapse time of the self-gravitating BEC as a function of its mass when started from $R_0 = 1$.

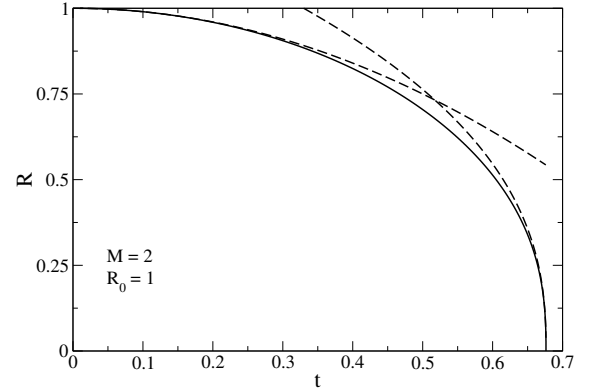


FIG. 15: Collapse of the self-gravitating BEC starting from $R_0 = 1$ for $M = 2$. The collapse time is $t_{\text{coll}} = 0.676301\dots$

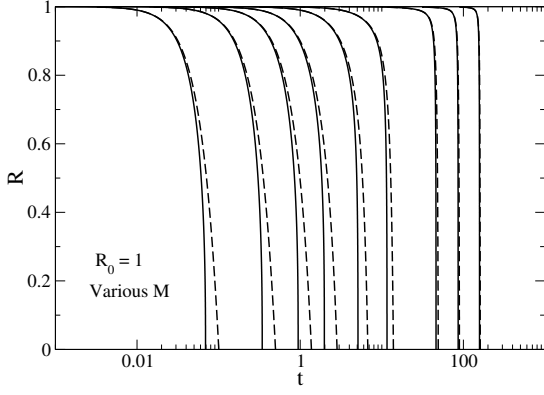


FIG. 16: Collapse of the self-gravitating BEC starting from $R_0 = 1$ for different values of the mass $M = 100, 5, 1.5, 1.1, 1.01, 1.001, 1.00001, 1.000001, 1.0000001$ (left to right). The dashed lines correspond to the invariant profile of Appendix C 3 [see Eq. (C25)] valid close to the critical point $M = 1$.

In particular, for $R_0 = 1$, we get

$$R(t) \simeq 1 - (M - 1)t^2. \quad (71)$$

C. Behavior of $R(t)$ for $t \rightarrow t_{\text{coll}}$

For $t \rightarrow t_{\text{coll}}$, corresponding to $R \rightarrow 0$, using the expression (43) of the potential, we can make the approximation

$$V(R_0) - V(R) \simeq \frac{M^2}{3R^3} \quad (72)$$

in Eq. (66). In this limit, the self-gravity and the quantum force are negligible with respect to the attractive self-interaction. Performing the integral in Eq. (66) with the approximation of Eq. (72), we obtain

$$R(t) \sim \left(\frac{25}{6}\right)^{1/5} M^{1/5} (t_{\text{coll}} - t)^{2/5}. \quad (73)$$

We note that this scaling is different from the scaling $R(t) \propto (t_{\text{coll}} - t)^{1/2}$ obtained by exactly solving the nongravitational GP equation with an attractive self-interaction [102]. This shows that the Gaussian ansatz is not always accurate.

D. Behavior of $t_{\text{coll}}(M, R_0)$ for $R_0 \rightarrow 0$

For fixed M and $R_0 \rightarrow 0$, we can neglect the quantum potential ($\propto 1/R^2$) and the self-gravity ($\propto 1/R$) in front of the self-interaction ($\propto 1/R^3$). In that case, Eq. (67) reduces to

$$t_{\text{coll}} \sim \sqrt{\frac{M}{2}} \int_0^{R_0} \frac{dR}{\sqrt{-\frac{M^2}{3R_0^3} + \frac{M^2}{3R^3}}}. \quad (74)$$

This can be rewritten as

$$t_{\text{coll}} \sim \sqrt{\frac{3}{2M}} R_0^{5/2} \int_0^1 \frac{dx}{\sqrt{\frac{1}{x^3} - 1}}. \quad (75)$$

Using

$$\int_0^1 \frac{dx}{\sqrt{\frac{1}{x^3} - 1}} = \frac{\sqrt{\pi} \Gamma(5/6)}{\Gamma(1/3)} = 0.746834\dots, \quad (76)$$

we obtain

$$t_{\text{coll}} \sim \sqrt{\frac{3\pi}{2}} \frac{\Gamma(5/6)}{\Gamma(1/3)} \frac{R_0^{5/2}}{\sqrt{M}} \sim 0.914681\dots \frac{R_0^{5/2}}{\sqrt{M}}. \quad (77)$$

E. Behavior of $t_{\text{coll}}(M, R_0)$ for $R_0 \rightarrow +\infty$

For fixed M and $R_0 \rightarrow +\infty$, we can neglect the quantum potential ($\propto 1/R^2$) and the self-interaction ($\propto 1/R^3$) in front of the self-gravity ($\propto 1/R$). In that case, Eq. (67) reduces to

$$t_{\text{coll}} \sim \sqrt{\frac{M}{2}} \int_0^{R_0} \frac{dR}{\sqrt{-\frac{M^2}{R_0} + \frac{M^2}{R}}}. \quad (78)$$

This can be rewritten as

$$t_{\text{coll}} \sim \frac{1}{\sqrt{2M}} R_0^{3/2} \int_0^1 \frac{dx}{\sqrt{\frac{1}{x} - 1}}. \quad (79)$$

Using

$$\int_0^1 \frac{dx}{\sqrt{\frac{1}{x} - 1}} = \frac{\pi}{2}, \quad (80)$$

we obtain

$$t_{\text{coll}} \sim \frac{\pi}{2\sqrt{2}} \frac{R_0^{3/2}}{\sqrt{M}} \sim 1.11072\dots \frac{R_0^{3/2}}{\sqrt{M}}. \quad (81)$$

V. THE THOMAS-FERMI LIMIT $M \rightarrow +\infty$

The limit $M \rightarrow +\infty$ corresponds to the TF approximation in which the quantum potential ($\propto M$) can be neglected in front of the self-gravity ($\propto M^2$) and the self-interaction ($\propto M^2$).

A. The evolution of the radius of the BEC

In the TF limit, the evolution of the radius of the BEC is given by

$$\int_{R(t)}^{R_0} \frac{dR}{\sqrt{-\frac{1}{3R_0^3} - \frac{1}{R_0} + \frac{1}{3R^3} + \frac{1}{R}}} = \sqrt{2Mt}. \quad (82)$$

This equation describes the collapse of the BEC under the action of the self-interaction and the self-gravity when $E_{\text{tot}} < 0$. If $R_0 \ll 1$, we can neglect the self-gravity in front of the self-interaction and we obtain

$$\int_{\frac{R(t)}{R_0}}^1 \frac{dx}{\sqrt{-1 + \frac{1}{x^3}}} = \sqrt{\frac{2M}{3R_0^5}} t. \quad (83)$$

This equation describes the collapse of the BEC under the action of the self-interaction alone when $E_{\text{tot}} < 0$ (this asymptotic limit $R_0 \ll 1$ is actually valid for all M). The integral has the analytical expression

$$\int_a^1 \frac{dx}{\sqrt{-1 + \frac{1}{x^3}}} = \frac{\sqrt{\pi}\Gamma(5/6)}{\Gamma(1/3)} - \frac{2}{5} a^{5/2} {}_2F_1\left(\frac{1}{2}, \frac{5}{6}, \frac{11}{6}, a^3\right). \quad (84)$$

Combining Eqs. (83) and (84), we obtain the evolution of the radius of the BEC under the form $t = t(R)$. If $R_0 \gg 1$, we can neglect the self-interaction in front of the self-gravity for sufficiently short times and we obtain

$$\int_{\frac{R(t)}{R_0}}^1 \frac{dx}{\sqrt{-1 + \frac{1}{x}}} = \sqrt{\frac{2M}{R_0^3}} t. \quad (85)$$

This equation describes the collapse of the BEC under the action of the self-gravity alone when $E_{\text{tot}} < 0$ (this asymptotic limit $R_0 \gg 1$ is actually valid for all M). The integral has the analytical expression

$$\int_a^1 \frac{dx}{\sqrt{-1 + \frac{1}{x}}} = \sqrt{a(1-a)} + \cos^{-1}(\sqrt{a}). \quad (86)$$

Combining Eqs. (85) and (86), we obtain the evolution of the radius of the BEC under the form $t = t(R)$. This solution, which describes the gravitational collapse of a homogeneous sphere with a negative energy $E_{\text{tot}} < 0$ was first found by Mestel [103]. It is usually written in parametric form as

$$R = R_0 \cos^2 \theta, \quad \sqrt{\frac{2M}{R_0^3}} t = \theta + \frac{1}{2} \sin(2\theta), \quad (87)$$

where θ is a parameter going from $\theta = 0$ to $\theta = \pi/2$ (collapse). This solution also occurs in cosmology. It describes the expansion, then the collapse, of a pressureless FLRW universe with curvature $k = +1$ [97]. It is usually written in parametric form as

$$R = \frac{1}{2} R_0 (1 - \cos \Theta), \quad \sqrt{\frac{2M}{R_0^3}} t = \frac{1}{2} (\Theta - \sin \Theta - \pi), \quad (88)$$

where Θ is a parameter going from $\Theta = 0$ (Big Bang) to $\Theta = 2\pi$ (Big Crunch) passing by $\Theta = \pi$ (maximum expansion). This is the equation of a cycloid. The solutions of Eqs. (87) and (88) are related to each other by the change of variables $\Theta = 2\theta + \pi$.

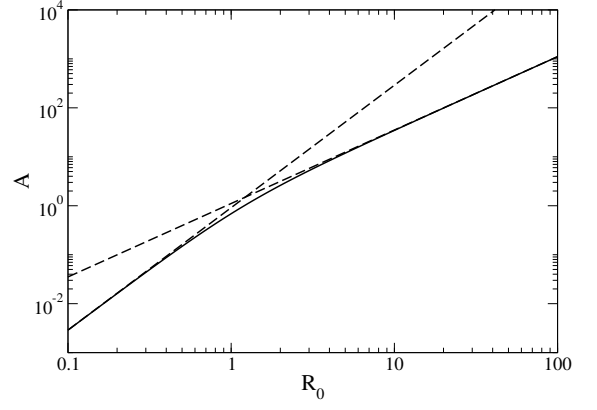


FIG. 17: The function $A(R_0)$.

B. Behavior of $t_{\text{coll}}(M, R_0)$ for $M \rightarrow +\infty$

In the TF limit, the expression of the collapse time given by Eq. (67) reduces to

$$t_{\text{coll}} \sim \frac{A(R_0)}{M^{1/2}} \quad (89)$$

with

$$A(R_0) = \frac{1}{\sqrt{2}} \int_0^{R_0} \frac{dR}{\sqrt{-\frac{1}{3R_0^3} - \frac{1}{R_0} + \frac{1}{3R^3} + \frac{1}{R}}}. \quad (90)$$

This function is plotted in Fig. 17. For $R_0 = 1$, we find $A(1) = 0.688033\dots$. For $R_0 \rightarrow 0$, we can neglect the self-gravity with respect to the self-interaction and obtain

$$A(R_0) \sim \sqrt{\frac{3\pi}{2}} \frac{\Gamma(5/6)}{\Gamma(1/3)} R_0^{5/2} \sim 0.914681\dots R_0^{5/2}, \quad (91)$$

where we have used Eq. (76). For $R_0 \rightarrow +\infty$, we can neglect the self-interaction with respect to the self-gravity and obtain

$$A(R_0) \sim \frac{\pi}{2\sqrt{2}} R_0^{3/2} \sim 1.11072\dots R_0^{3/2}, \quad (92)$$

where we have used Eq. (80). This result can also be directly obtained from Eq. (87) with $\theta = \pi/2$. The asymptotic limits $R_0 \rightarrow 0$ and $R_0 \rightarrow +\infty$ are actually valid for all M as shown in Secs. IV D and IV E.

VI. COLLAPSE OF THE BEC WHEN STARTED CLOSE TO THE CRITICAL POINT $M \rightarrow M_{\text{max}}^+$

A. The normal form of the potential

We consider the collapse of the BEC when $R_0 \rightarrow R_* = 1$ and $M \rightarrow M_{\text{max}}^+ = 1^+$. Since we are close to the critical

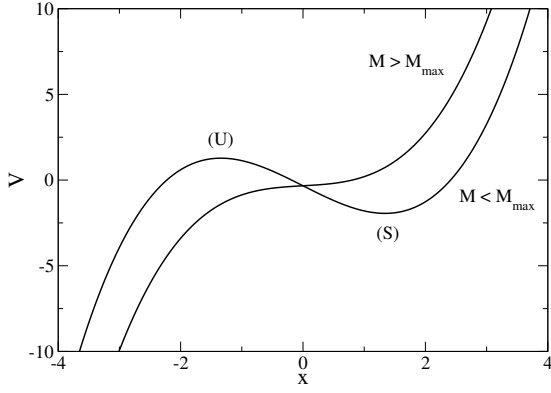


FIG. 18: Normal form of the effective potential close to the critical point corresponding to a saddle-node bifurcation.

point, corresponding to a saddle-node bifurcation, we can approximate the potential $V(R)$ by its normal form⁷

$$V(x) = -\frac{1}{3} - \frac{5}{3}(M-1) - 2(1-M)x + \frac{1}{3}x^3, \quad (93)$$

where we have written $x = R - 1$. This approximation is valid when $M \rightarrow 1$ and $x \ll 1$. The effective potential of Eq. (93) is plotted in Fig. 18 for illustration. In this approximation, for $M < M_{\max} = 1$, the equilibrium states, corresponding to $V'(x_e) = 0$, are given by $x_e = \pm\sqrt{2(1-M)}$. This returns the expression (50) of the mass-radius relation close to the critical point. We also recover the correct expression (57) of the total energy. On the other hand, $V''(x_e) = \pm 2\sqrt{2(1-M)}$. This immediately shows that the solution $x_e = +\sqrt{2(1-M)}$ is a minimum (stable) and the solution $x_e = -\sqrt{2(1-M)}$ is a maximum (unstable). Finally, the square of the complex pulsation is given by $\omega^2(x_e) = V''(x_e) = \pm 2\sqrt{2(1-M)}$ which returns the result of Eq. (61).

The equation of motion corresponding to the normal form (93) of the potential is

$$\frac{d^2x}{dt^2} = -V'(x) = 2(1-M) - x^2. \quad (94)$$

Its first integral is

$$E_{\text{tot}} = \frac{1}{2} \left(\frac{dx}{dt} \right)^2 + V(x). \quad (95)$$

We consider $M \geq 1$. Assuming $\dot{x} = 0$ and $x = x_0$ at $t = 0$, we obtain $E_{\text{tot}} = V(x_0)$ so that Eq. (95) yields

$$\frac{dx}{dt} = -\sqrt{2[V(x_0) - V(x)]}, \quad (96)$$

where the sign has been chosen so that $x(t)$ decreases with time since we are considering a collapse solution. Integrating this relation between 0 and t , we obtain

$$\int_{x(t)}^{x_0} \frac{dx}{\sqrt{2[V(x_0) - V(x)]}} = t. \quad (97)$$

Substituting the expression of $V(x)$ from Eq. (93) into Eq. (97), we get

$$\int_{x(t)}^{x_0} \frac{dx}{\sqrt{4(M-1)(x_0-x) + \frac{2}{3}(x_0^3-x^3)}} = t. \quad (98)$$

The effective particle released from x_0 without initial velocity ($\dot{x} = 0$) runs down the potential in the direction of increasingly negative values of x . The collapse time, corresponding to $x \rightarrow -\infty$, is given by

$$t_{\text{coll}} = \int_{-\infty}^{x_0} \frac{dx}{\sqrt{4(M-1)(x_0-x) + \frac{2}{3}(x_0^3-x^3)}}. \quad (99)$$

Using Eq. (99), we can rewrite Eq. (98) in the form

$$\int_{-\infty}^{x(t)} \frac{dx}{\sqrt{4(M-1)(x_0-x) + \frac{2}{3}(x_0^3-x^3)}} = t_{\text{coll}} - t. \quad (100)$$

For $t \rightarrow 0$, corresponding to $x \rightarrow x_0$, we can make the approximation $V(x) \simeq V(x_0) + V'(x_0)(x-x_0)$ so that Eq. (97) can be integrated into

$$x \simeq x_0 - \frac{1}{2}V'(x_0)t^2. \quad (101)$$

For the potential of Eq. (93), we get

$$x \simeq x_0 - \frac{1}{2}[2(M-1) + x_0^2]t^2. \quad (102)$$

This expression is consistent with the general result of Eq. (70) valid for *any* $M > 1$ and any R_0 . For $t \rightarrow t_{\text{coll}}$, corresponding to $x \rightarrow -\infty$, we can make the approximation $V(x_0) - V(x) \simeq -x^3/3$ so that Eq. (97) can be integrated into

$$x \sim -\frac{6}{(t_{\text{coll}} - t)^2}. \quad (103)$$

The evolution of the radius of the BEC $x(t; M, x_0)$ given by Eq. (98) and the collapse time $t_{\text{coll}}(M, x_0)$ given by Eq. (99) can be put in a self-similar form as shown in Appendix C and illustrated in Figs. 29, 30, 33 and in Figs. 28, 31, 32.

B. The case $M = 1$ and $R_0 \rightarrow 1$

For $M = 1$, the collapse time diverges when $R_0 \rightarrow 1$ because the effective potential given by Eq. (43) presents

⁷ The terms $-(4/3)(M-1)^2$, $2(M-1)^2x$ and $-3(M-1)x^2$ in the potential turn out to be always subdominant in our applications so, for simplicity, we do not consider them.

an inflexion point at $R = 1$ when $M = 1$. From Eq. (99), we obtain

$$t_{\text{coll}}(M = 1, R_0) \sim \sqrt{\frac{3}{2}} \int_{-\infty}^{x_0} \frac{dx}{\sqrt{x_0^3 - x^3}}. \quad (104)$$

Assuming $x_0 > 0$ and making the change of variables $y = x/x_0$, we get

$$t_{\text{coll}}(M = 1, R_0) \sim \sqrt{\frac{3}{2}} \frac{1}{x_0^{1/2}} \int_{-\infty}^1 \frac{dy}{\sqrt{1 - y^3}}. \quad (105)$$

Therefore, when $R_0 \rightarrow 1^+$:

$$t_{\text{coll}}(M = 1, R_0) \sim K_+(R_0 - 1)^{-1/2} \quad (106)$$

with

$$K_+ = \sqrt{\frac{3}{2}} \int_{-\infty}^1 \frac{dy}{\sqrt{1 - y^3}} = \sqrt{\frac{3\pi}{2}} \frac{\Gamma(1/3)}{\Gamma(5/6)} = 5.15195... \quad (107)$$

Assuming $x_0 < 0$ and making the change of variables $y = x/|x_0|$, we get

$$t_{\text{coll}}(M = 1, R_0) \sim \sqrt{\frac{3}{2}} \frac{1}{|x_0|^{1/2}} \int_{-\infty}^{-1} \frac{dy}{\sqrt{-1 - y^3}}. \quad (108)$$

Therefore, when $R_0 \rightarrow 1^-$:

$$t_{\text{coll}}(M = 1, R_0) \sim K_-(1 - R_0)^{-1/2} \quad (109)$$

with

$$K_- = \sqrt{\frac{3}{2}} \int_{-\infty}^{-1} \frac{dy}{\sqrt{-1 - y^3}} = \sqrt{6\pi} \frac{\Gamma(7/6)}{\Gamma(2/3)} = 2.97448... \quad (110)$$

C. The case $R_0 = 1$ and $M \rightarrow 1^+$

For $R_0 = 1$, the collapse time diverges when $M \rightarrow 1^+$ because the effective potential given by Eq. (43) presents an inflexion point at $R = 1$ when $M = 1$. From Eq. (99), we obtain

$$t_{\text{coll}}(M, R_0 = 1) = \int_{-\infty}^0 \frac{dx}{\sqrt{-4(M-1)x - \frac{2}{3}x^3}}. \quad (111)$$

Making the change of variables $y = x/\sqrt{6(M-1)}$, we find that the collapse time is given, when $M \rightarrow 1^+$, by

$$t_{\text{coll}}(M, R_0 = 1) \sim B(M-1)^{-1/4} \quad (112)$$

with

$$B = \left(\frac{3}{8}\right)^{1/4} \int_{-\infty}^0 \frac{dy}{\sqrt{-y - y^3}} \\ = \left(\frac{3}{8}\right)^{1/4} \int_{-\infty}^0 \frac{du}{\sqrt{-\sinh(u)}} = 2.90178... \quad (113)$$

To get the second line, we have made the change of variables $y = \sinh(u)$. For $M > M_{\text{max}}$, the collapse time diverges at the critical point as $t_{\text{coll}} \sim 2.90178...(M-1)^{-1/4}$. Interestingly, this is the same scaling as for the divergence of the period of the oscillations $2\pi/\omega \sim 3.73600...(1-M)^{-1/4}$ close to the critical point for $M < M_{\text{max}}$ [see Eq. (61)]. The prefactor is, however, different being 2.90178... for t_{coll} ($M > M_{\text{max}}$) and 3.73600... for $2\pi/\omega$ ($M < M_{\text{max}}$).

D. The Painlevé equation

If the mass M of the system increases with time as $M(t) = 1 + at/2$ (for example by accreting matter around it or because of a continuous inflow of particles), the equation of motion (94) can be rewritten as

$$\frac{d^2x}{dt^2} = -at - x^2, \quad (114)$$

where the origin of times has been chosen such that $M \leq M_{\text{max}}$ for $t \leq 0$ and $M \geq M_{\text{max}}$ for $t \geq 0$. In this way, an initially stable system loses its stability at $t = 0$ and collapses. Equation (114) is the celebrated Painlevé I equation. It has been studied in detail in [104] in a model of supernovae that presents a saddle-center bifurcation similar to our system.

VII. POSSIBLE COLLAPSE, EXPLOSION AND OSCILLATIONS OF THE BEC WHEN $M < M_{\text{max}}$

A. The critical mass M_c

When $M < M_{\text{max}}$, the effective potential is plotted in Figs. 19 and 20. The (local) maximum of the potential $V(R)$ corresponds to the energy of the unstable equilibrium state: $V_{\text{max}} = V(R_U) = E_{\text{tot}}(R_U)$. According to Eq. (55), V_{max} is positive when $R_U < R_c$ with

$$R_c = \frac{1}{\sqrt{3}} = 0.57735... \quad (115)$$

From Eq. (47), this corresponds to a mass $M < M_c$ with

$$M_c = \frac{\sqrt{3}}{2} = 0.866025... \quad (116)$$

This is a new critical mass that has not been introduced before. Restoring the dimensional variables, we have $M_c = 0.9396\hbar/\sqrt{Gm|a_s|}$ and $R_{99}^c = 2.382(|a_s|\hbar^2/Gm^3)^{1/2}$. For standard axions with $m = 10^{-4}$ eV/ c^2 and $a_s = -5.8 \cdot 10^{-53}$ m, we obtain $M_c = 5.98 \times 10^{-14} M_\odot$ and $R_c = 5.8 \times 10^{-5} R_\odot$. For ultra-light axions with $m = 1.93 \times 10^{-20}$ eV/ c^2 and $a_s = -8.29 \times 10^{-60}$ fm, we obtain $M_c = 3.62 \times 10^5 M_\odot$ and $R_c = 6$ pc.

When $M_c < M < M_{\text{max}}$, the local maximum of the effective potential is negative: $V_{\text{max}} < 0$ (see Fig. 19).

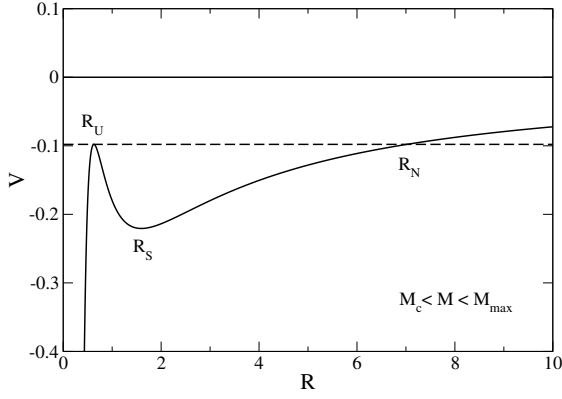


FIG. 19: Effective potential $V(R)$ as a function of the radius R for $M_c < M = 0.9 < M_{\max}$. In that case $V_{\max} < 0$.

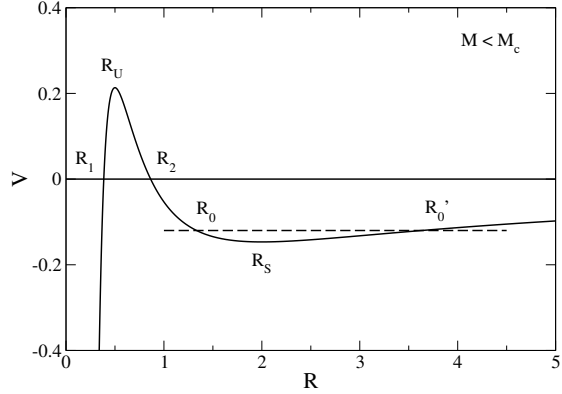


FIG. 20: Effective potential $V(R)$ as a function of the radius R for $M = 0.8 < M_c$. In that case $V_{\max} > 0$.

If $R_0 < R_U$, the BEC collapses. If $R_U < R < R_N$ where $R_N(M)$ is such that $V(R_N) = V(R_U)$ the BEC oscillates about its stable equilibrium state corresponding to $R = R_S$. If $R > R_N$, the BEC collapses. When slightly perturbed, the unstable equilibrium state at R_U (unstable branch) with $E_{\max} < 0$ can either collapse to a black hole or oscillate about the stable equilibrium at R_S .

When $M < M_c$, the local maximum of the effective potential is positive: $V_{\max} > 0$ (see Fig. 20). In that case, we introduce the radii R_1 and $R_2 > R_1$ at which the effective potential vanishes: $V(R_1) = V(R_2) = 0$. They are given by

$$R_1 = \frac{1 - \sqrt{1 - \left(\frac{M}{M_c}\right)^2}}{2M}, \quad (117)$$

$$R_2 = \frac{1 + \sqrt{1 - \left(\frac{M}{M_c}\right)^2}}{2M}. \quad (118)$$

If $R_0 < R_U$, the BEC collapses. If $R_U < R \leq R_2$, the

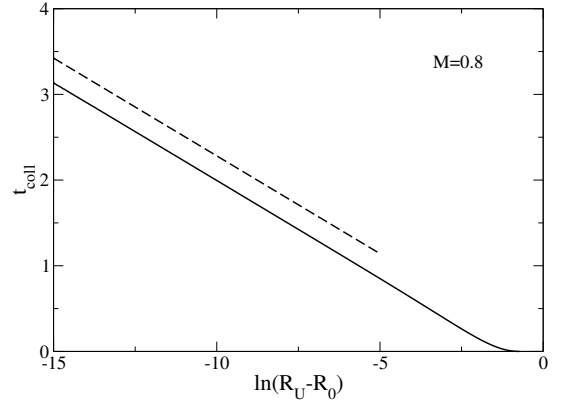


FIG. 21: Collapse time of the BEC when $R_0 \rightarrow R_U^-$ (we have taken $M = 0.8$). The dashed line corresponds to the asymptotic expression of Eq. (122).

BEC explodes. If $R > R_2$, the BEC oscillates about its stable equilibrium state corresponding to $R = R_S$. When slightly perturbed, the unstable equilibrium state at R_U (unstable branch) with $E_{\max} > 0$ can either collapse to a black hole or explode and disperse away.

B. Collapse of the BEC

1. Collapse time when $R_0 \rightarrow R_U^-$

When $R_0 < R_U$, the BEC collapses. The results of Sec. IV still apply. The collapse time diverges when $R_0 \rightarrow R_U^-$ because the effective potential given by Eq. (43) presents a maximum at R_U . Writing $R_0 = R_U - x_0$ and $R = R_U - x$, expanding Eq. (65) for $x_0 \ll 1$ and $x \ll 1$, and using $V'(R_U) = 0$ and $V''(R_U) < 0$, we obtain

$$t_{\text{coll}} \sim \sqrt{\frac{M}{-V''(R_U)}} \int_{x_0}^{R_U} \frac{dx}{\sqrt{x^2 - x_0^2}}. \quad (119)$$

Making the change of variables $y = x/x_0$, we get

$$t_{\text{coll}} \sim \sqrt{\frac{M}{-V''(R_U)}} \int_1^{R_U/x_0} \frac{dy}{\sqrt{y^2 - 1}}. \quad (120)$$

Using

$$\int_1^z \frac{dy}{\sqrt{y^2 - 1}} = \ln(z + \sqrt{z^2 - 1}), \quad (121)$$

we obtain for $R_0 \rightarrow R_U^-$:

$$t_{\text{coll}} \sim -\sqrt{\frac{M}{-V''(R_U)}} \ln\left(\frac{R_U - R_0}{2R_U}\right). \quad (122)$$

The divergence is logarithmic. The collapse time is plotted as a function of $\ln(R_U - R_0)$ in Fig. 21, and compared

with the asymptotic result of Eq. (122). This formula is only valid at leading order which explains the offset with the exact solution on this figure.

Remark: For $M = M_c$, we have $R_U = 1/\sqrt{3}$ and $V''(R_U) = -9\sqrt{3}/2$.

2. Collapse time when $M_c < M < M_{\max}$ and $R_0 \rightarrow R_N^+$

We consider the case $M_c < M < M_{\max}$. When $R_0 > R_N$, the BEC collapses. The results of Sec. IV still apply. The collapse time diverges when $R_0 \rightarrow R_N^+$ because the effective potential given by Eq. (43) presents a maximum at R_U . Therefore, the effective particle takes an infinitely long time to reach that maximum before collapsing. Writing $R_0 = R_N + \epsilon$ and $R = R_U + x$, expanding Eq. (65) for $\epsilon \ll 1$ and $x \ll 1$, and using $V'(R_U) = 0$, $V''(R_U) < 0$ and $V'(R_N) > 0$, we obtain

$$t_{\text{coll}} \sim \sqrt{\frac{M}{2}} \int_{-R_U}^{R_N - R_U + \epsilon} \frac{dx}{\sqrt{V'(R_N)\epsilon - V''(R_U)\frac{x^2}{2}}}. \quad (123)$$

Making the change of variables

$$y = \sqrt{\frac{-V''(R_U)}{2V'(R_N)\epsilon}} x, \quad (124)$$

we get

$$t_{\text{coll}} \sim \sqrt{\frac{M}{-V''(R_U)}} \int_{-R_U}^{(R_N - R_U)\sqrt{\frac{-V''(R_U)}{2V'(R_N)\epsilon}}} \frac{dy}{\sqrt{1 + y^2}}. \quad (125)$$

Using

$$\int \frac{dy}{\sqrt{1 + y^2}} = \sinh^{-1}(y), \quad (126)$$

the foregoing equation can be rewritten as

$$t_{\text{coll}} \sim \sqrt{\frac{M}{-V''(R_U)}} \left\{ \sinh^{-1} \left[(R_N - R_U) \sqrt{\frac{-V''(R_U)}{2V'(R_N)\epsilon}} \right] + \sinh^{-1} \left(R_U \sqrt{\frac{-V''(R_U)}{2V'(R_N)\epsilon}} \right) \right\}. \quad (127)$$

Using the equivalent $\sinh^{-1}(y) \sim \ln(2y)$ valid for $y \rightarrow +\infty$, we finally obtain

$$t_{\text{coll}} \sim \sqrt{\frac{M}{-V''(R_U)}} \ln \left[-\frac{4(R_N - R_U)R_U V''(R_U)}{2V'(R_N)(R_0 - R_N)} \right]. \quad (128)$$

The divergence is logarithmic. This formula is only valid at leading order.

Remark: For $M \rightarrow M_c$, we have $R_U \rightarrow 1/\sqrt{3}$, $V''(R_U) \rightarrow -9\sqrt{3}/2$, $R_N \sim M_c^2/[3(M - M_c)]$ and $V'(R_N) \sim 9(M - M_c)^2/M_c^2$. To obtain these asymptotic results, we have used $R_U \simeq 1/\sqrt{3} + (4/3)(M - M_c)$, $V(R_U) \sim -3(M - M_c)$ for $M \rightarrow M_c$ and $V(R) \sim -M^2/R$ for $R \rightarrow +\infty$.

C. Explosion of the BEC

We consider the case $M < M_c$. We assume $R_U < R_0 \leq R_2$ and $\dot{R}_0 = 0$ (implying $E_{\text{tot}} = V(R_0)$) leading to the explosion of the BEC. In that case, according to Eq. (46), the evolution of the radius $R(t)$ of the BEC is given by

$$\int_{R_0}^{R(t)} \frac{dR}{\sqrt{V(R_0) - V(R)}} = \left(\frac{2}{M} \right)^{1/2} t, \quad (129)$$

where the sign has been chosen so that $R(t)$ increases with time since we are considering an explosive solution.

1. Behavior of $R(t)$ for $t \rightarrow 0$

For $t \rightarrow 0$, corresponding to $R \rightarrow R_0$, we can make the approximation $V(R) \simeq V(R_0) + V'(R_0)(R - R_0)$ with $V'(R_0) < 0$ so that Eq. (129) becomes

$$\int_{R_0}^{R(t)} \frac{dR}{\sqrt{-V'(R_0)(R - R_0)}} = \left(\frac{2}{M} \right)^{1/2} t \quad (130)$$

leading to

$$R(t) \simeq R_0 - \frac{1}{2M} V'(R_0) t^2. \quad (131)$$

For the potential of Eq. (43), Eq. (131) takes the form

$$R(t) \simeq R_0 - \frac{1}{2} \left[-\frac{2}{R_0^3} + \frac{M}{R_0^4} + \frac{M}{R_0^2} \right] t^2. \quad (132)$$

2. Behavior of $R(t)$ for $t \rightarrow +\infty$ when $R_U < R_0 < R_2$

We assume $R_U < R_0 < R_2$. For $t \rightarrow +\infty$, corresponding to $R \rightarrow +\infty$, the potential $V(R) \rightarrow 0$. In this limit, the effective particle has a free motion so that, at leading order, Eq. (129) leads to

$$R(t) \sim \sqrt{\frac{2V(R_0)}{M}} t. \quad (133)$$

It possible to take into account the other terms in the potential $V(R)$ perturbatively. For late times, the effective potential is dominated by the gravity term: $V(R) \sim -M^2/R$. Therefore, we can rewrite Eq. (129) as

$$\int_{R_0}^{R(t)} \frac{dR}{\sqrt{V(R_0) + \frac{M^2}{R}}} \simeq \left(\frac{2}{M} \right)^{1/2} t \quad (134)$$

and treat the gravitational term as a small correction. We get

$$R(t) - \frac{M^2}{2V(R_0)} \ln R(t) \simeq \sqrt{\frac{2V(R_0)}{M}} t, \quad (135)$$

leading to

$$R(t) \simeq \sqrt{\frac{2V(R_0)}{M}} t + \frac{M^2}{2V(R_0)} \ln \left[\sqrt{\frac{2V(R_0)}{M}} t \right]. \quad (136)$$

This result can also be obtained by evaluating the integral in Eq. (134) with the identity

$$\int \frac{dx}{\sqrt{1 + \frac{a}{x}}} = \sqrt{x(a+x)} - a \ln(\sqrt{x} + \sqrt{a+x}) \quad (137)$$

and taking the limit $R \rightarrow +\infty$. The temporal evolution of the radius of the BEC is shown in Fig. 22. Equation (134) describes the explosion of a homogeneous self-gravitating sphere with positive energy $E_{\text{tot}} > 0$. Combining Eqs. (134) and (137), we obtain the evolution of the radius of the system under the form $t = t(R)$. This solution also occurs in cosmology. It describes the expansion of a pressureless FLRW universe with curvature $k = -1$ [97]. It is usually written in parametric form as

$$\frac{V(R_0)}{M^2} R(t) = \frac{1}{2} (\cosh \Psi - 1), \quad (138)$$

$$\frac{V(R_0)}{M^2} \sqrt{\frac{2V(R_0)}{M}} t = \frac{1}{2} (\sinh \Psi - \Psi - \sinh \Psi_0 + \Psi_0), \quad (139)$$

where Ψ is a parameter going from Ψ_0 to $+\infty$.

Remark: One can check that the correction due to the quantum potential is not divergent when $t \rightarrow +\infty$ so the asymptotic result of Eq. (136) cannot be improved.

3. Behavior of $R(t)$ for $t \rightarrow +\infty$ when $R_0 = R_2$

We assume that $R_0 = R_2$. In that case $E_{\text{tot}} = V(R_0) = 0$ so the equation of motion reduces to

$$\int_{R_2}^{R(t)} \frac{dR}{\sqrt{-\frac{M}{R^2} + \frac{M^2}{3R^3} + \frac{M^2}{R}}} = \left(\frac{2}{M}\right)^{1/2} t. \quad (140)$$

For $t \rightarrow +\infty$, corresponding to $R \rightarrow +\infty$, the effective potential is dominated by the gravity term. We obtain at leading order

$$R(t) \sim \left(\frac{9}{2}M\right)^{1/3} t^{2/3}. \quad (141)$$

This solution describes the explosion of a homogeneous self-gravitating sphere with vanishing energy $E_{\text{tot}} = 0$.

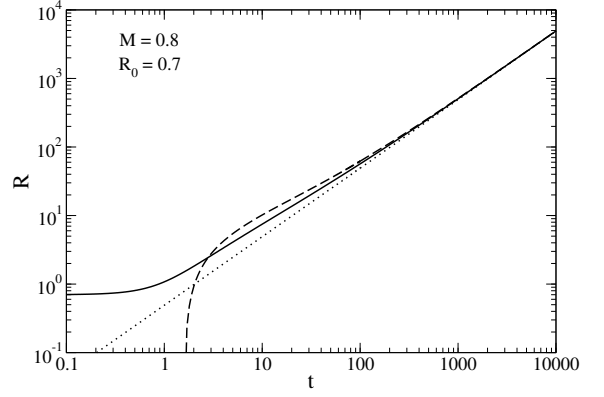


FIG. 22: Explosion of the BEC for $M = 0.8 < M_c$ and $R_0 < R_2$ (for this initial radius $V(R_0) = 0.0964025$). The dotted line corresponds to the asymptotic expression given by Eq. (133) and the dashed line corresponds to the asymptotic expression given by Eq. (136).

This solution also occurs in cosmology. It describes the expansion of a pressureless FLRW universe without curvature ($k = 0$) [97]. This is the famous Einstein-de Sitter (EdS) solution. The $t^{2/3}$ behavior of $R(t)$ in Eq. (141) when $E_{\text{tot}} = 0$ can be contrasted from its linear behavior in Eq. (133) when $E_{\text{tot}} > 0$.

We can take into account the correction coming from the quantum potential perturbatively. We start from the equation

$$\int_{R_2}^{R(t)} \frac{dR}{\sqrt{-\frac{M}{R^2} + \frac{M^2}{R}}} \simeq \left(\frac{2}{M}\right)^{1/2} t \quad (142)$$

and treat the quantum potential as a small correction. We obtain

$$R(t) \simeq \left(\frac{9}{2}M\right)^{1/3} t^{2/3} \left[1 - \left(\frac{2}{9}\right)^{1/3} \frac{1}{M^{4/3}} \frac{1}{t^{2/3}} \right]. \quad (143)$$

This result can also be obtained by evaluating the integral in Eq. (142) with the identity

$$\int \frac{dx}{\sqrt{-\frac{1}{x^2} + \frac{a}{x}}} = \frac{2}{3a^2} (2+ax) \sqrt{ax-1} \quad (144)$$

and taking the limit $R \rightarrow +\infty$. The temporal evolution of the radius of the BEC is shown in Fig. 23. We note that Eq. (142) describes the explosion of the BEC under the action of the quantum potential and the self-gravity when $E_{\text{tot}} = 0$. Combining Eqs. (142) and (144), we obtain the evolution of the radius of the BEC in that case under the form $t = t(R)$.

Remark: One can check that the correction due to the self-interaction is not divergent when $t \rightarrow +\infty$ so the asymptotic result of Eq. (143) cannot be improved.

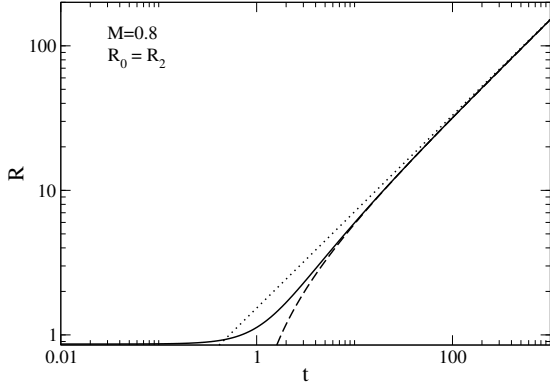


FIG. 23: Explosion of the BEC for $M = 0.8 < M_c$ and $R_0 = R_2 = 0.86436\dots$ (for this initial radius $V(R_0) = 0$). The dotted line corresponds to the asymptotic expression given by Eq. (141) and the dashed line corresponds to the asymptotic expression given by Eq. (143).

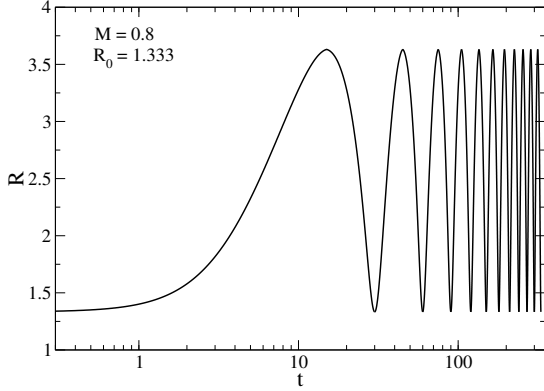


FIG. 24: Oscillations of the BEC for $M = 0.8 < M_c$ and $R_0 = 1.333$ (for this initial radius $V(R_0) = -0.12$).

D. Oscillations of the BEC

In certain cases, the BEC oscillates. When $M_c < M < M_{\max}$, this happens when $R_U < R_0 < R_N$. When $M < M_c$, this happens when $R_0 > R_2$. The period of the oscillations is given by

$$T = \pm \sqrt{2M} \int_{R_0}^{R'_0} \frac{dR}{\sqrt{V(R_0) - V(R)}}, \quad (145)$$

where R'_0 is determined by the condition $V(R'_0) = V(R_0)$. The sign $+$ corresponds to $R_0 < R'_0$ and the sign $-$ corresponds to $R_0 > R'_0$. The BEC oscillates about the equilibrium radius R_S , between the extremal radii R_0 and R'_0 . The pulsation is $\omega = 2\pi/T$. The oscillations of the BEC are illustrated in Fig. 24.

1. The oscillations close to equilibrium

Close to the minimum R_S , the effective potential can be approximated by the quadratic form $V(R) = V(R_S) + (1/2)V''(R_S)(R - R_S)^2$. In that case $R'_0 = 2R_S - R_0$. Making the change of variables $x = (R - R_S)/(R_S - R_0)$, we find that the period of the oscillations is given by

$$T = \sqrt{\frac{4M}{V''(R_S)}} \int_{-1}^{+1} \frac{dx}{\sqrt{1-x^2}}. \quad (146)$$

Using

$$\int_{-1}^{+1} \frac{dx}{\sqrt{1-x^2}} = \pi, \quad (147)$$

we obtain

$$T = 2\pi \sqrt{\frac{M}{V''(R_S)}}. \quad (148)$$

This returns the result of Eq. (59).

2. The case $M_c < M < M_{\max}$ and $R_0 \rightarrow R_U^+$

We consider the case $M_c < M < M_{\max}$. The period of the oscillations diverges when $R_0 \rightarrow R_U^+$ because the effective potential given by Eq. (43) presents a maximum at R_U . Writing $R_0 = R_U + x_0$ and $R = R_U + x$, expanding Eq. (145) for $x_0 \ll 1$ and $x \ll 1$, and using $V'(R_U) = 0$ and $V''(R_U) < 0$, we obtain

$$T \simeq \sqrt{\frac{4M}{-V''(R_U)}} \int_{x_0}^{R_N - R_U} \frac{dx}{\sqrt{x^2 - x_0^2}}. \quad (149)$$

Making the change of variables $y = x/x_0$, we get

$$T \simeq \sqrt{\frac{4M}{-V''(R_U)}} \int_1^{(R_N - R_U)/x_0} \frac{dy}{\sqrt{y^2 - 1}}. \quad (150)$$

Using Eq. (121), we obtain for $R_0 \rightarrow R_U^+$:

$$T \sim \sqrt{\frac{4M}{-V''(R_U)}} \ln \left(2 \frac{R_N - R_U}{R_0 - R_U} \right). \quad (151)$$

The divergence is logarithmic. This expression can be compared with the expression (122) of the collapse time of the BEC when $R_0 \rightarrow R_U^-$.

When $R_0 \rightarrow R_U^+$, R'_0 can be deduced from the relation

$$R_0 - R_U = \sqrt{\frac{2V'(R_N)(R'_0 - R_N)}{V''(R_U)}} \quad (152)$$

obtained by equating $V(R_0) \simeq V(R_U) + (1/2)V''(R_U)(R_0 - R_U)^2$ and $V(R'_0) \simeq V(R_N) +$

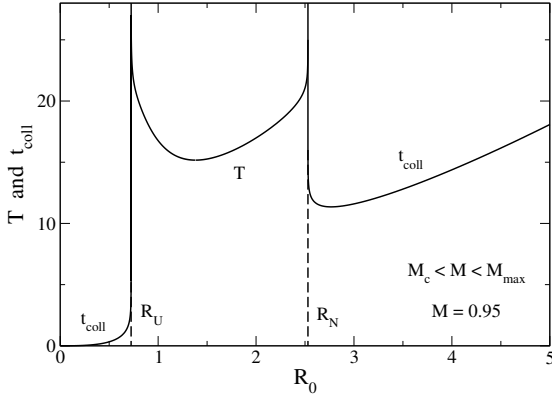


FIG. 25: Period of the oscillations of the BEC as a function of $R_0 \in [R_U, R_N]$ when $M_c < M < M_{\max}$ (we have taken $M = 0.95$). The period of the oscillations diverges according to Eq. (151) for $R_0 \rightarrow R_U^+$ and according to Eq. (153) for $R_0 \rightarrow R_N^-$. Its minimum is given by Eq. (148). We have also represented the collapse time for $R_0 < R_U$ and $R_0 > R_N$. It diverges according to Eq. (122) for $R_0 \rightarrow R_U^-$ and according to Eq. (128) for $R_0 \rightarrow R_N^+$. It tends to 0 for $R_0 \rightarrow 0$ according to Eq. (77) and to $+\infty$ for $R_0 \rightarrow +\infty$ according to Eq. (81).

$V'(R_N)(R'_0 - R_N)$, and using $V(R_U) = V(R_N)$. If we start from $R_0 \rightarrow R_N^-$, the period of the oscillations is given by Eq. (151) with the substitution of Eq. (152) and the final replacement of R'_0 by R_0 . This gives

$$T \sim \sqrt{\frac{M}{-V''(R_U)}} \ln \left[\frac{2V''(R_U)(R_N - R_U)^2}{V'(R_N)(R_0 - R_N)} \right]. \quad (153)$$

The formulae (151) and (153) are only valid at leading order. These results are illustrated in Fig. 25.

Remark: the expressions of the different quantities appearing in Eqs. (151) and (153) when $M \rightarrow M_c$ have been given at the end of Sec. VII B 2.

3. The case $M < M_c$ and $R_0 \rightarrow R_2^+$

We consider the case $M < M_c$. When $R_0 \rightarrow R_2^+$, R'_0 is rejected to infinity. For large values of R , the effective potential can be approximated by $V(R) \sim -M^2/R$. Writing $V(R_0) \simeq V'(R_2)(R_0 - R_2)$ and $V(R'_0) \simeq -M^2/R'_0$, the condition $V(R'_0) = V(R_0)$ gives

$$R'_0 \sim \frac{M^2}{|V'(R_2)|(R_0 - R_2)}. \quad (154)$$

When $R_0 \rightarrow R_2^+$, Eq. (145) can be approximated by

$$T \simeq \sqrt{2M} \int_{R_0}^{R'_0} \frac{dR}{\sqrt{V(R_0) + \frac{M^2}{R}}}. \quad (155)$$

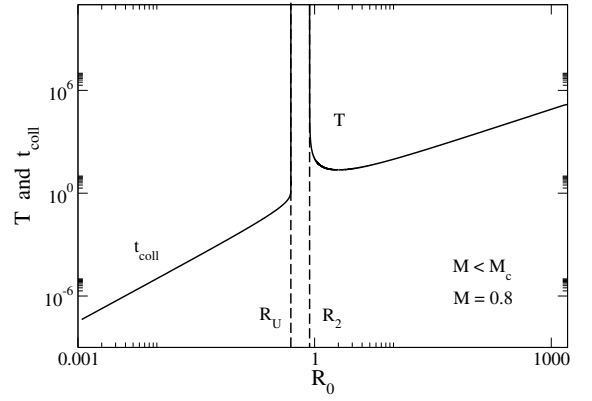


FIG. 26: Period of the oscillations of the BEC as a function of $R_0 \geq R_2$ when $M < M_c$ (we have taken $M = 0.8$). The period of the oscillations diverges according to Eq. (158) for $R_0 \rightarrow R_2^+$ and according to Eq. (159) for $R_0 \rightarrow +\infty$. Its minimum is given by Eq. (148). We have also represented the collapse time of the BEC as a function of $R_0 \leq R_U$. It diverges according to Eq. (122) for $R_0 \rightarrow R_U^-$. It tends to 0 for $R_0 \rightarrow 0$ according to Eq. (77).

Writing $V(R_0) \simeq V'(R_2)(R_0 - R_2)$, we obtain

$$T \simeq \sqrt{\frac{2M}{|V'(R_2)|(R_0 - R_2)}} \times \int_{R_0}^{R'_0} \frac{dR}{\sqrt{-1 + \frac{M^2}{R|V'(R_2)|(R_0 - R_2)}}}. \quad (156)$$

Making the change of variables $x = R|V'(R_2)|(R_0 - R_2)/M^2$, we get

$$T \sim \frac{\sqrt{2}M^{5/2}}{|V'(R_2)|^{3/2}(R_0 - R_2)^{3/2}} \int_0^1 \frac{dx}{\sqrt{\frac{1}{x} - 1}}. \quad (157)$$

Using the identity (80), we find that, when $R_0 \rightarrow R_2^+$, the period of the oscillations is given by

$$T \sim \frac{\pi M^{5/2}}{\sqrt{2}|V'(R_2)|^{3/2}(R_0 - R_2)^{3/2}}. \quad (158)$$

If we start from $R_0 \rightarrow +\infty$, the period of the oscillations is given by Eq. (158) with the substitution of Eq. (154) and the final replacement of R'_0 by R_0 . This gives

$$T \sim \frac{\pi}{\sqrt{2M}} R_0^{3/2}. \quad (159)$$

These results are illustrated in Fig. 26.

Remark: For $M \rightarrow M_c$, we have $R_2 \simeq 1/\sqrt{3} + (2/3^{3/4})\sqrt{M_c - M}$, and $V'(R_2) \sim -3^{7/4}\sqrt{M_c - M}$.

VIII. THE LIMIT $M \rightarrow 0$

In this section, we investigate the limit $M \rightarrow 0$. In this limit,

$$R_U \sim \frac{M}{2}, \quad R_S \sim \frac{2}{M}, \quad (160)$$

$$V(R_U) \sim \frac{4}{3M}, \quad V(R_S) \sim -\frac{M^3}{4}, \quad (161)$$

$$R_1 \sim \frac{M}{3}, \quad R_2 \sim \frac{1}{M}. \quad (162)$$

The expressions of R_U , $V(R_U)$ and R_1 for $M \rightarrow 0$ can be obtained by neglecting the gravitational term in the effective potential (43). This corresponds to the nongravitational limit. The expressions of R_S , $V(R_S)$ and R_2 for $M \rightarrow 0$ can be obtained by neglecting the self-interaction term in the effective potential (43). This corresponds to the noninteracting limit.

A. The nongravitational limit $M \rightarrow 0$ and $R \sim M \ll 1$

For $M \rightarrow 0$ and $R \sim M \ll 1$, we can neglect the gravitational term in the effective potential (43). According to Eq. (46), the evolution of the radius of the BEC is given by

$$\int_{R(t)}^{R_0} \frac{dR}{\sqrt{\frac{M}{R_0^2} - \frac{M^2}{3R_0^3} - \frac{M}{R^2} + \frac{M^2}{3R^3}}} = \pm \left(\frac{2}{M}\right)^{1/2} t, \quad (163)$$

where the sign + corresponds to a contraction of the BEC and the sign - corresponds to an expansion of the BEC. Since we assume $R \sim M$, we define $R_0 = qM$. With the change of variables $x = R/M$, the foregoing equation can be rewritten as

$$\int_{\frac{R(t)}{M}}^q \frac{dx}{\sqrt{\frac{1}{q^2} - \frac{1}{3q^3} - \frac{1}{x^2} + \frac{1}{3x^3}}} = \pm \frac{\sqrt{2}}{M^2} t. \quad (164)$$

This equation describes the evolution of the BEC under the action of the self-interaction and the quantum potential for any E_{tot} .

We consider the collapse of the BEC starting from $R_0 \leq R_U$. This corresponds to $q \leq 1/2$. The collapse time, obtained from the condition $R(t_{\text{coll}}) = 0$, is given by

$$t_{\text{coll}}(M, R_0) = f\left(\frac{R_0}{M}\right) M^2 \quad (165)$$

with

$$f(q) = \frac{1}{\sqrt{2}} \int_0^q \frac{dx}{\sqrt{\frac{1}{q^2} - \frac{1}{3q^3} - \frac{1}{x^2} + \frac{1}{3x^3}}}. \quad (166)$$

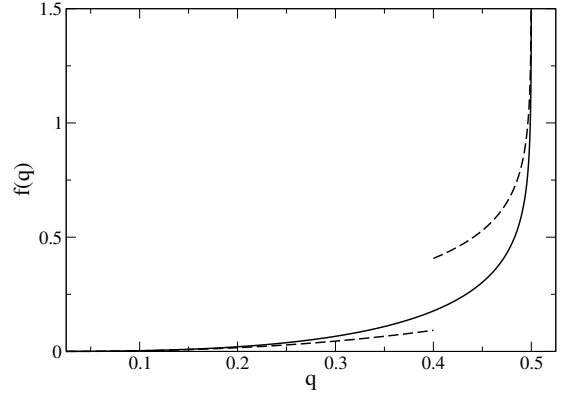


FIG. 27: The function $f(q)$. The dashed lines correspond to the asymptotic behaviors given by Eqs. (167) and (168).

This function is plotted in Fig. 27. For $q \rightarrow 0$, using Eq. (76), we get

$$f(q) \sim \sqrt{\frac{3\pi}{2}} \frac{\Gamma(5/6)}{\Gamma(1/3)} q^{5/2}. \quad (167)$$

Substituting this asymptotic result in Eq. (165), we recover Eq. (77). For $q \rightarrow 1/2$, using Eq. (121), we get

$$f(q) \sim -\frac{1}{4\sqrt{2}} \ln\left(\frac{1}{2} - q\right). \quad (168)$$

Substituting this asymptotic result in Eq. (165), we recover Eq. (122) with $R_U \sim M/2$ and $V''(R_U) \sim -32/M^3$. For $R_0 = R_1$, corresponding to $q = 1/3$, we have $E_{\text{tot}} = V(R_0) = 0$. Using the identity

$$\int_s^{1/3} \frac{dx}{\sqrt{-\frac{1}{x^2} + \frac{1}{3x^3}}} = \frac{1}{12} \left[(1+2s)\sqrt{3s(1-3s)} + \cos^{-1}(\sqrt{3s}) \right], \quad (169)$$

we find that Eq. (164) with the sign + (collapse) becomes

$$\frac{1}{12} \left[\left(1 + \frac{2R}{M}\right) \sqrt{\frac{3R}{M} \left(1 - \frac{3R}{M}\right)} + \cos^{-1}\left(\sqrt{\frac{3R}{M}}\right) \right] = \frac{\sqrt{2}}{M^2} t. \quad (170)$$

This equation describes the collapse of the BEC under the action of the self-interaction and the quantum potential when $E_{\text{tot}} = 0$. On the other hand, using $f(1/3) = \pi/24\sqrt{2}$, the collapse time is exactly given by

$$t_{\text{coll}}(M, R_0 = R_1) = \frac{\pi}{24\sqrt{2}} M^2. \quad (171)$$

This expression is valid for sufficiently small values of M so that the self-gravity of the BEC can be neglected.

Remark: if we assume $E_{\text{tot}} = 0$ and neglect the quantum potential in Eq. (163), we obtain

$$R(t) = R_0 \left(1 - \frac{5}{\sqrt{6}} \frac{M^{1/2}}{R_0^{5/2}} t \right)^{2/5}, \quad (172)$$

leading to

$$t_{\text{coll}} = \frac{\sqrt{6}}{5} \frac{R_0^{5/2}}{M^{1/2}}. \quad (173)$$

Equation (172) describes the collapse of the BEC with $E_{\text{tot}} = 0$ under the action of the self-interaction alone (the explosive solution is obtained from Eq. (172) by changing the sign $-$ into $+$). Taking $R_0 = M/3$, we get $t_{\text{coll}} = \sqrt{2}M^2/45$ which is different by a factor ~ 3 from Eq. (171) obtained by taking the quantum potential into account.

B. The noninteracting limit $M \rightarrow 0$ and $R \sim 1/M \gg 1$

For $M \rightarrow 0$ and $R \sim 1/M \gg 1$, we can neglect the self-interaction in the effective potential (43). According to Eq. (46), the evolution of the radius of the BEC is given by

$$\int_{R_0}^{R(t)} \frac{dR}{\sqrt{\frac{M}{R_0^2} - \frac{M^2}{R_0} - \frac{M}{R^2} + \frac{M^2}{R}}} = \pm \left(\frac{2}{M} \right)^{1/2} t, \quad (174)$$

where the sign $+$ corresponds to an expansion of the BEC and the sign $-$ corresponds to a contraction of the BEC. Since we assume $R \sim 1/M$, we define $R_0 = q/M$. With the change of variables $x = RM$, the foregoing equation can be rewritten as

$$\int_q^{MR(t)} \frac{dx}{\sqrt{\frac{1}{q^2} - \frac{1}{q} - \frac{1}{x^2} + \frac{1}{x}}} = \pm \sqrt{2}M^2 t. \quad (175)$$

This equation describes the evolution of the BEC under the action of the self-gravity and the quantum potential for any E_{tot} . The integral can be calculated analytically using the identity

$$\int \frac{dx}{\sqrt{a - \frac{1}{x^2} + \frac{1}{x}}} = \frac{1}{a} \sqrt{ax^2 + x - 1} - \frac{1}{2a^{3/2}} \ln \left[1 + 2ax + 2\sqrt{a} \sqrt{ax^2 + x - 1} \right]. \quad (176)$$

Combining Eqs. (175) and (176), we can obtain an analytical expression of the evolution of the radius of the BEC under the form $t = t(R)$. For $R_0 = R_2$, corresponding to $q = 1$, we have $E_{\text{tot}} = V(R_0) = 0$. In that case, using the identity

$$\int \frac{dx}{\sqrt{-\frac{1}{x^2} + \frac{1}{x}}} = \frac{2}{3}(2+x)\sqrt{x-1}, \quad (177)$$

we find that Eq. (174) with the sign $+$ becomes

$$\frac{2}{3}(2+MR)\sqrt{MR-1} = \sqrt{2}M^2 t. \quad (178)$$

This equation describes the explosion of the BEC under the action of the self-gravity and the quantum potential when $E_{\text{tot}} = 0$.

Equation (174) describe the evolution of the BEC under the action of the quantum potential and the self-gravity. For sufficiently small values of R_0 and sufficiently short times, self-gravity can be neglected and Eq. (174) reduces to

$$\int_{R_0}^{R(t)} \frac{dR}{\sqrt{\frac{M}{R_0^2} - \frac{M}{R^2}}} = \left(\frac{2}{M} \right)^{1/2} t. \quad (179)$$

This equation describes the explosion of the BEC under the action of the quantum potential alone. It can be integrated into

$$R = R_0 \sqrt{1 + \frac{2t^2}{R_0^4}}. \quad (180)$$

IX. CONCLUSION

In this paper, we have completed our previous investigations [27, 28] concerning self-gravitating BECs with attractive self-interaction ($a_s < 0$). Axions generally have an attractive self-interaction so they enter in the framework of our study. Standard axions can coalesce into axion stars. Axion stars are stable only if their mass does not exceed a certain maximum mass [see Eq. (1)] obtained in [27, 28]. In general, this mass is extremely small. The question then arises to what happens to an axion star with a mass larger than M_{max} ? In this paper, we have considered the possibility that the star collapses and forms a black hole. We have used a Newtonian model based on the GPP equations and, using a Gaussian ansatz, we have determined an approximate expression of the collapse time at which the star collapses to a point. We have obtained the analytical asymptotic behaviors

$$\frac{t_{\text{coll}}}{t_D} \sim \frac{0.688033\dots}{(M/M_{\text{max}})^{1/2}}, \quad (M \gg M_{\text{max}}), \quad (181)$$

$$\frac{t_{\text{coll}}}{t_D} \sim \frac{2.90178\dots}{(M/M_{\text{max}} - 1)^{1/4}}, \quad (M \rightarrow M_{\text{max}}^+), \quad (182)$$

where M_{max} is the maximum mass of a stable axion star and t_D is the dynamical time. For a standard axion particle with $m = 10^{-4} \text{ eV}/c^2$ and $a_s = -5.8 \cdot 10^{-53} \text{ m}$, we have $M_{\text{max}} = 6.9 \times 10^{-14} M_{\odot}$, $R_* = 1.0 \times 10^{-4} R_{\odot}$ and $t_D = 3.4 \text{ hrs}$. From our general expression of the collapse time [see Eq. (67)], an axion star with a mass $M = 2M_{\text{max}} = 1.4 \times 10^{-13} M_{\odot}$ and an initial radius $R_0 = R_* = 1.0 \times 10^{-4} R_{\odot}$ will form a mini black hole of

mass $M = 1.4 \times 10^{-13} M_\odot$ in a time $t_{\text{coll}} = 0.676301 t_D = 2.3$ hrs. This time is very short. Therefore, if dark matter is made of standard axions, they could be in the form of mini black holes instead of mini axion stars. Of course, our Newtonian treatment is only valid as long as the radius of the star is much larger than its Schwarzschild radius. When the radius of the star approaches its Schwarzschild radius, general relativity must be taken into account in order to describe the formation of a black hole. However, we have shown in Appendix E that general relativistic effects become important only extraordinarily close to the collapse time ($\Delta t = 1.09 \times 10^{-32}$ s for standard axions) so our Newtonian treatment is justified. We have also considered the case of ultralight axions which may cluster into dark matter halos. For ultralight axions with $m = 1.93 \times 10^{-20}$ eV/ c^2 and $a_s = -8.29 \times 10^{-60}$ fm, we obtain $M_{\text{max}} = 4.18 \times 10^5 M_\odot$, $R_* = 10.4$ pc, and $t_D = 1.49$ Myrs. An axionic dark matter halo with a mass $M = 2M_{\text{max}} = 8.36 \times 10^5 M_\odot$ and an initial radius $R_0 = R_* = 10.4$ pc will form a supermassive black hole of mass $M = 8.36 \times 10^5 M_\odot$ (similar to those reported at the center of galaxies) in a time $t_{\text{coll}} = 0.676301 t_D = 1.01$ Myrs. General relativistic effects become important only $\Delta t = 8.47 \times 10^{-8}$ s before the collapse time.

In addition to the black hole scenario, other possibilities can be considered as recently discussed by Braaten *et al.* [62] in the case of axion stars. The first possibility is that the collapse of the axion star can be accompanied by a burst of relativistic axions produced by inelastic reactions when the density reaches high values. This would lead to a bosonova. A similar phenomenon has been observed in the collapse of a (non-gravitational) BEC of ultracold atoms with an attractive self-interaction [105]. The emission of relativistic axions could decrease the mass of the axion star so that it always remains larger than its Schwarzschild radius. Another possibility is that an axion star with $M > M_{\text{max}}$ loses mass by emitting scalar field radiation through the process of gravitational cooling [89]. In this manner, its core mass M_{core} always remains smaller than M_{max} , avoiding its catastrophic collapse into a black hole. An axion star with $M > M_{\text{max}}$ may also fragmentate into several pieces of mass $M' < M_{\text{max}}$. There is also the possibility of forming dense axion stars. The stable axions stars that we have considered in [27, 28] are dilute axion stars in which the self-gravity and the attractive self-interaction are balanced by the quantum force (kinetic energy). As proposed by Braaten *et al.* [62], there may exist dense axion stars in which gravity is balanced by the pressure of the axion condensate coming from higher order terms in the scalar field potential $V(\phi)$ beyond the $\lambda\phi^4$ term. This leads to a sequence of new branches of axion stars. The first branch of these dense axion stars has mass ranging from about $10^{-11} M_\odot$ to about M_\odot .

On a technical point of view, our study provides a lot of analytical results concerning the collapse, the explosion, and the oscillations of self-gravitating BECs with nega-

tive scattering length. As already mentioned, our analytical results are based on a Gaussian ansatz that may not always be quantitatively reliable. It would be therefore interesting to compare our analytical results with an exact numerical solution of the GPP equations. On the other hand, we have used a fully Newtonian model although the system becomes relativistic at the end of the collapse, when it approaches the Schwarzschild radius. Therefore, one should solve the KGE equations to have a more exact description of the dynamics. These are interesting problems for the future. However, the richness of the problem already revealed by our simple analytical study shows that the full numerical simulation of the GPP and KGE equations, and their study, will require a considerable amount of work.

Appendix A: Derivation of the GP equation from the KG equation

In this Appendix, we show that the GP equation can be derived from the KG equation in the nonrelativistic limit $c \rightarrow +\infty$ and we relate the scattering length a_s appearing in the GP equation to the self-interaction constant λ appearing in the KG equation. We follow the procedure of [52, 53]. The KG equation for a complex scalar field ϕ writes

$$\frac{1}{c^2} \frac{\partial^2 \phi}{\partial t^2} - \Delta \phi + \frac{m^2 c^2}{\hbar^2} \left(1 + \frac{2\Phi}{c^2} \right) \phi + 2 \frac{dV}{d|\phi|^2} \phi = 0, \quad (\text{A1})$$

where $V = V(|\phi|^2)$ is the self-interaction potential of the SF and Φ is an external potential that, in a simplified model, can be identified with the gravitational potential (see [52, 53] for a fully general relativistic treatment). The KG equation without self-interaction can be viewed as the relativistic generalization of the Schrödinger equation. Similarly, the KG equation with a self-interaction can be viewed as the relativistic generalization of the GP equation. In order to recover the Schrödinger and GP equations in the nonrelativistic limit $c \rightarrow +\infty$, we make the Klein transformation⁸

$$\phi(\mathbf{r}, t) = \frac{\hbar}{m} e^{-imc^2 t/\hbar} \psi(\mathbf{r}, t), \quad (\text{A2})$$

where ψ is the wave function. The rest-mass density is given by $\rho = |\psi|^2 = (m/\hbar)^2 |\phi|^2$. Substituting Eq. (A2) into the KG equation (A1), we get

$$\frac{\hbar^2}{2mc^2} \frac{\partial^2 \psi}{\partial t^2} - i\hbar \frac{\partial \psi}{\partial t} - \frac{\hbar^2}{2m} \Delta \psi + m\Phi\psi + m \frac{dV}{d|\psi|^2} \psi = 0. \quad (\text{A3})$$

Taking the nonrelativistic limit $c \rightarrow +\infty$ of Eq. (A3), we obtain the nonlinear Schrödinger equation

$$i\hbar \frac{\partial \psi}{\partial t} = -\frac{\hbar^2}{2m} \Delta \psi + m\Phi\psi + m \frac{dV}{d|\psi|^2} \psi. \quad (\text{A4})$$

⁸ The prefactor is derived in [52, 53].

It can be written as a GP equation of the form

$$i\hbar \frac{\partial \psi}{\partial t} = -\frac{\hbar^2}{2m} \Delta \psi + m\Phi \psi + mh(|\psi|^2)\psi \quad (\text{A5})$$

with a nonlinearity

$$h(|\psi|^2) = \frac{dV}{d|\psi|^2} \quad \text{i.e.} \quad h(\rho) = V'(\rho). \quad (\text{A6})$$

As we have recalled in footnote 4, the GP equation with a cubic nonlinearity (corresponding to $h(\rho) \propto \rho$) can be derived from the mean field Schrödinger equation with a pair contact potential. The present approach shows that the GP equation with an *arbitrary* nonlinearity $h(\rho)$ can be derived from the KG equation with an arbitrary self-interaction potential $V(\rho)$: the potential $h(\rho)$ determining the nonlinearity in the GP equation is equal to the derivative of the potential $V(\rho)$ in the KG equation; reciprocally, $V(\rho)$ is a primitive of $h(\rho)$.

The potential $h(\rho)$ determining the nonlinearity in the standard GP equation (7) is

$$h = \frac{4\pi a_s \hbar^2}{m^3} \rho. \quad (\text{A7})$$

According to Eq. (A6), it corresponds to a potential of the form

$$V = \frac{2\pi a_s \hbar^2}{m^3} \rho^2 = \frac{2\pi a_s m}{\hbar^2} |\phi|^4. \quad (\text{A8})$$

With this potential, the KG equation (A1) explicitly writes

$$\frac{1}{c^2} \frac{\partial^2 \phi}{\partial t^2} - \Delta \phi + \frac{m^2 c^2}{\hbar^2} \left(1 + \frac{2\Phi}{c^2}\right) \phi + \frac{8\pi a_s m}{\hbar^2} |\phi|^2 \phi = 0. \quad (\text{A9})$$

Therefore, a cubic nonlinearity in the GP equation corresponds to a quartic potential in the KG equation. In general, the quartic potential is written in the form

$$V(|\phi|^2) = \frac{\lambda}{4\hbar c} |\phi|^4, \quad (\text{A10})$$

where λ is a dimensionless self-interaction constant. Comparison between (A8) and (A10) yields

$$\frac{\lambda}{8\pi} = \frac{a_s m c}{\hbar}. \quad (\text{A11})$$

This justifies Eq. (B9) of [27].

The pressure appearing in the quantum Euler equation associated with the GP equation is due to the self-interaction of the bosons. It is given in terms of the potential V by [27]:

$$P(\rho) = \rho V'(\rho) - V(\rho). \quad (\text{A12})$$

For the quartic potential (A8), we get Eq. (18), i.e. a polytropic equation of state of index $n = 1$. More generally, for a power-law potential of the form

$$V(|\phi|^2) = \frac{K}{\gamma - 1} \left(\frac{m}{\hbar}\right)^{2\gamma} |\phi|^{2\gamma}, \quad (\text{A13})$$

we get the polytropic equation of state

$$P = K\rho^\gamma, \quad \gamma = 1 + \frac{1}{n}. \quad (\text{A14})$$

In particular, for a sextic potential $V(|\phi|^2) = (K/2)(m/\hbar)^6 |\phi|^6$ (which is the term coming after the quartic potential), we obtain $P = K\rho^3$, i.e. a polytropic equation of state of index $n = 1/2$.

Appendix B: Lagrangian of a self-gravitating BEC

In this Appendix, we discuss the Lagrangian structure of the GPP equations and of the corresponding hydrodynamic equations. The Lagrangian of the GPP equation is

$$L = \int \left\{ \frac{i\hbar}{2m} \left(\psi^* \frac{\partial \psi}{\partial t} - \psi \frac{\partial \psi^*}{\partial t} \right) - \frac{\hbar^2}{2m^2} |\nabla \psi|^2 - \frac{1}{2} \Phi |\psi|^2 - \frac{2\pi a_s \hbar^2}{m^3} |\psi|^4 \right\} d\mathbf{r}. \quad (\text{B1})$$

We can view the Lagrangian (B1) as a functional of ψ , $\dot{\psi}$ and $\nabla \psi$. The action is $S = \int L dt$. The least action principle $\delta S = 0$, which is equivalent to the Lagrange equation

$$\frac{\partial}{\partial t} \left(\frac{\delta L}{\delta \dot{\psi}} \right) + \nabla \cdot \left(\frac{\delta L}{\delta \nabla \psi} \right) - \frac{\delta L}{\delta \psi} = 0, \quad (\text{B2})$$

returns the GP equation (7). The total energy is obtained from the transformation

$$E_{\text{tot}} = \int \frac{i\hbar}{2m} \left(\psi^* \frac{\partial \psi}{\partial t} - \psi \frac{\partial \psi^*}{\partial t} \right) d\mathbf{r} - L \quad (\text{B3})$$

leading to

$$E_{\text{tot}} = \int \frac{\hbar^2}{2m^2} |\nabla \psi|^2 d\mathbf{r} + \int \frac{1}{2} \Phi |\psi|^2 d\mathbf{r} + \int \frac{2\pi a_s \hbar^2}{m^3} |\psi|^4 d\mathbf{r}. \quad (\text{B4})$$

The first term is the kinetic energy, the second term is the gravitational energy and the third term is the self-interaction energy. Using the Lagrange equations, one can show that the total energy is conserved. On the other hand, the GP equation (7) can be written as

$$i\hbar \frac{\partial \psi}{\partial t} = m \frac{\delta E_{\text{tot}}}{\delta \psi^*}. \quad (\text{B5})$$

This expression directly implies the conservation of the total energy E_{tot} . From general arguments [96], a minimum of energy E_{tot} under the normalization condition $\int |\psi|^2 d\mathbf{r} = M$ is a stationary solution of the GP equation that is formally nonlinearly dynamically stable. Writing the variational principle as

$$\delta E_{\text{tot}} - \frac{\mu}{m} \delta \int |\psi|^2 d\mathbf{r} = 0, \quad (\text{B6})$$

where μ is a Lagrange multiplier (chemical potential), we recover the time-independent GP equation (9) with $E = \mu$. This shows that the chemical potential μ can be identified with the eigenenergy E , or reciprocally.

Using the Madelung transformation, we can rewrite the Lagrangian in terms of hydrodynamic variables. According to Eqs. (10) and (11) we have

$$\frac{\partial S}{\partial t} = -i\frac{\hbar}{2} \frac{1}{|\psi|^2} \left(\psi^* \frac{\partial \psi}{\partial t} - \psi \frac{\partial \psi^*}{\partial t} \right) \quad (\text{B7})$$

and

$$|\nabla\psi|^2 = \frac{1}{4\rho} (\nabla\rho)^2 + \frac{\rho}{\hbar^2} (\nabla S)^2. \quad (\text{B8})$$

Substituting these identities in Eq. (B1) we get

$$L = - \int \left\{ \frac{\rho}{m} \frac{\partial S}{\partial t} + \frac{\rho}{2m^2} (\nabla S)^2 + \frac{\hbar^2}{8m^2} \frac{(\nabla\rho)^2}{\rho} + \frac{1}{2} \rho\Phi + \frac{2\pi a_s \hbar^2}{m^3} \rho^2 \right\} d\mathbf{r}. \quad (\text{B9})$$

We can view the Lagrangian (B9) as a functional of S , \dot{S} , ∇S , ρ , $\dot{\rho}$, and $\nabla\rho$. The Lagrange equation for the action

$$\frac{\partial}{\partial t} \left(\frac{\delta L}{\delta \dot{S}} \right) + \nabla \cdot \left(\frac{\delta L}{\delta \nabla S} \right) - \frac{\delta L}{\delta S} = 0 \quad (\text{B10})$$

returns the equation of continuity (13). The Lagrange equation for the density

$$\frac{\partial}{\partial t} \left(\frac{\delta L}{\delta \dot{\rho}} \right) + \nabla \cdot \left(\frac{\delta L}{\delta \nabla \rho} \right) - \frac{\delta L}{\delta \rho} = 0 \quad (\text{B11})$$

returns the quantum Hamilton-Jacobi (or Bernoulli) equation (14) leading to the quantum Euler equation (15). The total energy is obtained from the transformation

$$E_{\text{tot}} = - \int \frac{\rho}{m} \frac{\partial S}{\partial t} d\mathbf{r} - L \quad (\text{B12})$$

leading to

$$E_{\text{tot}} = \int \frac{1}{2} \rho \mathbf{u}^2 d\mathbf{r} + \int \frac{\hbar^2}{8m^2} \frac{(\nabla\rho)^2}{\rho} d\mathbf{r} + \frac{1}{2} \int \rho\Phi d\mathbf{r} + \int \frac{2\pi a_s \hbar^2}{m^3} \rho^2 d\mathbf{r}. \quad (\text{B13})$$

The first term is the classical kinetic energy, the second term is the quantum kinetic energy (or quantum potential energy), the third term is the gravitational energy, and the fourth term is the self-interaction energy. Using the Lagrange equations, one can show that the total energy is conserved. Therefore, a stable stationary solution of the EP equations is a minimum of energy E_{tot} under the mass constraint $M = \int \rho d\mathbf{r}$. Writing the variational principle as

$$\delta E_{\text{tot}} - \frac{\mu}{m} \delta M = 0, \quad (\text{B14})$$

where μ is a Lagrange multiplier (chemical potential), we recover Eq. (19). Taking its gradient, we recover the condition of hydrostatic equilibrium (20) [27].

With the Gaussian ansatz of Eq. (22), one has

$$\begin{aligned} & \int \frac{i\hbar}{2m} \left(\psi^* \frac{\partial \psi}{\partial t} - \psi \frac{\partial \psi^*}{\partial t} \right) d\mathbf{r} \\ &= - \int \frac{\rho}{m} \frac{\partial S}{\partial t} d\mathbf{r} = -\frac{1}{2} \alpha M R^2 \dot{H} \end{aligned} \quad (\text{B15})$$

and

$$\begin{aligned} E_{\text{tot}} &= \frac{1}{2} \alpha M R^2 H^2 + \sigma \frac{\hbar^2 M}{m^2 R^2} \\ &+ \zeta \frac{2\pi a_s \hbar^2 M^2}{m^3 R^3} - \nu \frac{GM^2}{R}. \end{aligned} \quad (\text{B16})$$

Substituting these expressions in Eq. (B3) or in Eq. (B12), we obtain the effective Lagrangian

$$\begin{aligned} L(H, \dot{H}, R) &= -\frac{1}{2} \alpha M R^2 (\dot{H} + H^2) - \sigma \frac{\hbar^2 M}{m^2 R^2} \\ &- \zeta \frac{2\pi a_s \hbar^2 M^2}{m^3 R^3} + \nu \frac{GM^2}{R}. \end{aligned} \quad (\text{B17})$$

We can view the Lagrangian (B17) as a function of H , \dot{H} and R . The Lagrange equation for H

$$\frac{\partial}{\partial t} \left(\frac{\delta L}{\delta \dot{H}} \right) - \frac{\delta L}{\delta H} = 0 \quad (\text{B18})$$

returns Eq. (26). The Lagrange equation for R

$$\frac{\delta L}{\delta R} = 0 \quad (\text{B19})$$

returns the equation of motion (29). We also note that, using Eq. (26), the total energy can be written as

$$\begin{aligned} E_{\text{tot}} &= \frac{1}{2} \alpha M \left(\frac{dR}{dt} \right)^2 + \sigma \frac{\hbar^2 M}{m^2 R^2} \\ &+ \zeta \frac{2\pi a_s \hbar^2 M^2}{m^3 R^3} - \nu \frac{GM^2}{R}, \end{aligned} \quad (\text{B20})$$

leading to Eqs. (27) and (28).

Appendix C: Self-similar solutions close to the critical point $M \rightarrow M_{\text{max}}^+$ and $R_0 \rightarrow R_*$

For $M \rightarrow M_{\text{max}}^+$ and $R_0 \rightarrow R_*$, the temporal evolution of the radius $R(t; M, R_0)$ of the BEC and the collapse time $t_{\text{coll}}(M, R_0)$ have a self-similar structure. This self-similar structure can be directly obtained from the normal form of the effective potential close to the critical point given by Eq. (93). This corresponds to a saddle node bifurcation.

1. Self-similar solution with a normalization by $R_0 > R_*$

The temporal evolution of the radius of the BEC is determined by Eq. (98). We first consider the case $x_0 > 0$. Making the change of variables $y = x/x_0$ and introducing the scaled variables

$$T = \sqrt{\frac{2}{3}} x_0^{1/2} t, \quad X(T) = \frac{x(t)}{x_0}, \quad \mu = \frac{6(M-1)}{x_0^2}, \quad (\text{C1})$$

where t , $x(t)$ and M are normalized in terms of x_0 , we can rewrite Eq. (98) as

$$\int_{X(T)}^1 \frac{dy}{\sqrt{\mu(1-y) + 1 - y^3}} = T. \quad (\text{C2})$$

The collapse time, corresponding to $X \rightarrow -\infty$, is given by

$$T_{\text{coll}}(\mu) = \int_{-\infty}^1 \frac{dy}{\sqrt{\mu(1-y) + 1 - y^3}}. \quad (\text{C3})$$

With the scaled variables, the collapse dynamics of the BEC close to the critical point depends on a single parameter μ instead of the two parameters M and x_0 . For $\mu = 0$, we get

$$\int_{X(T)}^1 \frac{dy}{\sqrt{1 - y^3}} = T \quad (\text{C4})$$

and

$$\begin{aligned} T_{\text{coll}}(\mu = 0) &= \int_{-\infty}^1 \frac{dy}{\sqrt{1 - y^3}} \\ &= \sqrt{\pi} \frac{\Gamma(1/3)}{\Gamma(5/6)} = 4.20655\dots \end{aligned} \quad (\text{C5})$$

In the general case, returning to the original variables, we obtain for $R_0 > 1$:

$$\frac{t_{\text{coll}}(M, R_0)}{t_{\text{coll}}(M=1, R_0)} = f_+ \left[\frac{6(M-1)}{(R_0-1)^2} \right] \quad (\text{C6})$$

with

$$f_+(\mu) = \frac{\int_{-\infty}^1 \frac{dy}{\sqrt{\mu(1-y) + 1 - y^3}}}{\int_{-\infty}^1 \frac{dy}{\sqrt{1 - y^3}}} \quad (\text{C7})$$

and

$$t_{\text{coll}}(M=1, R_0) = K_+(R_0 - 1)^{-1/2}, \quad (\text{C8})$$

where K_+ is given by Eq. (107). The invariant profile defined by Eq. (C7) behaves as

$$f_+(\mu) \sim \frac{6^{1/4} B}{K_+} \mu^{-1/4} \sim 0.881517\dots \mu^{-1/4} \quad (\text{C9})$$

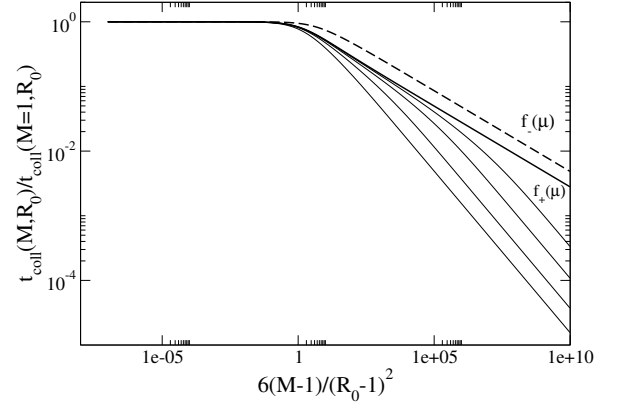


FIG. 28: Evolution of the collapse time $M \mapsto t_{\text{coll}}(M, R_0)$ in scaled variables. We have taken $R_0 = 1.1, 1.01, 1.001, 1.0001$ (bottom to top). The rescaled profile converges towards the invariant profile $f_+(\mu)$ when $R_0 \rightarrow 1^+$ and $M \rightarrow 1$. It has an asymptotic logarithmic slope $-1/4$. For $M \gg 1$, the self-similar solution is not valid anymore and the collapse time behaves according to Eq. (89) with a logarithmic slope $-1/2$. The two slopes are clearly visible on the figure. For comparison, we have also represented the invariant profile $f_-(\mu)$ corresponding to $R_0 < 1$ (see Sec. C2).

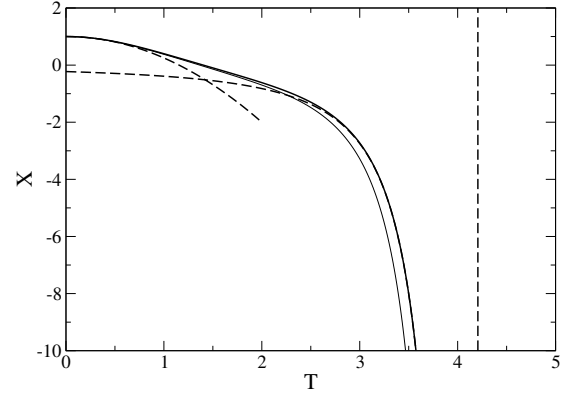


FIG. 29: Universal evolution of the scaled radius of the BEC $X(T; \mu)$ close to the critical point corresponding to a saddle-node bifurcation. The thick curve corresponds to $\mu = 0$. According to the results of Secs. IV B and IV C, we have $X \sim 1 - 3T^2/4$ for $T \rightarrow 0$ and $X \sim -4/(T_{\text{coll}} - T)^2$ for $T \rightarrow T_{\text{coll}} = 4.20655\dots$. The thin curve corresponds to $\mu = 0.1$.

for $\mu \rightarrow +\infty$.

The exact collapse time given by Eq. (67) is plotted in scaled variables in Fig. 28 in order to illustrate its convergence towards the invariant profile given by Eq. (C7) as $R_0 \rightarrow 1^+$ and $M \rightarrow 1^+$. The universal evolution of the radius of the BEC in scaled variables given by Eq. (C2), valid close to the critical point, is plotted in Fig. 29.

Remark: The integral of Eq. (C4) has the analytical

expression

$$\int_X^1 \frac{dy}{\sqrt{1-y^3}} = \frac{\sqrt{\pi}\Gamma(4/3)}{\Gamma(5/6)} - X {}_2F_1\left(\frac{1}{3}, \frac{1}{2}, \frac{4}{3}, X^3\right). \quad (\text{C10})$$

2. Self-similar solution with a normalization by

$$R_0 < R_*$$

We now consider the case $x_0 < 0$. Making the change of variables $y = x/|x_0|$, and introducing the scaled variables

$$T = \sqrt{\frac{2}{3}}|x_0|^{1/2}t, \quad X(T) = \frac{x(t)}{|x_0|}, \quad \mu = \frac{6(M-1)}{x_0^2}, \quad (\text{C11})$$

where t , $x(t)$ and M are normalized in terms of x_0 , we can rewrite Eq. (98) as

$$\int_{X(T)}^{-1} \frac{dy}{\sqrt{\mu(-y-1)-y^3-1}} = T. \quad (\text{C12})$$

The collapse time, corresponding to $X \rightarrow -\infty$, is given by

$$T_{\text{coll}}(\mu) = \int_{-\infty}^{-1} \frac{dy}{\sqrt{\mu(-y-1)-y^3-1}}. \quad (\text{C13})$$

With the scaled variables, the collapse dynamics of the BEC close to the critical point depends on a single parameter μ instead of the two parameters M and R_0 . For $\mu = 0$, we get

$$\int_{X(T)}^{-1} \frac{dy}{\sqrt{-y^3-1}} = T \quad (\text{C14})$$

and

$$\begin{aligned} T_{\text{coll}}(\mu = 0) &= \int_{-\infty}^{-1} \frac{dy}{\sqrt{-y^3-1}} \\ &= 2\sqrt{\pi} \frac{\Gamma(7/6)}{\Gamma(2/3)} = 2.42865\dots \end{aligned} \quad (\text{C15})$$

In the general case, returning to the original variables, we obtain for $R_0 < 1$:

$$\frac{t_{\text{coll}}(M, R_0)}{t_{\text{coll}}(M = 1, R_0)} = f_- \left[\frac{6(M-1)}{(1-R_0)^2} \right] \quad (\text{C16})$$

with

$$f_-(\mu) = \frac{\int_{-\infty}^{-1} \frac{dy}{\sqrt{\mu(-y-1)-y^3-1}}}{\int_{-\infty}^{-1} \frac{dy}{\sqrt{-y^3-1}}} \quad (\text{C17})$$

and

$$t_{\text{coll}}(M = 1, R_0) = K_-(1-R_0)^{-1/2}, \quad (\text{C18})$$

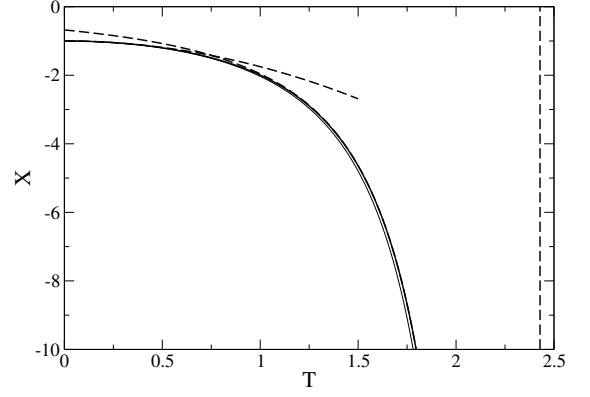


FIG. 30: Universal evolution of the scaled radius of the BEC $X(T; \mu)$ close to the critical point corresponding to a saddle-node bifurcation. The thick curve corresponds to $\mu = 0$. According to the results of Secs. IV B and IV C, we have $X \sim -1 - 3T^2/4$ for $T \rightarrow 0$ and $X \sim -4/(T_{\text{coll}} - T)^2$ for $T \rightarrow T_{\text{coll}} = 2.42865\dots$. The thin curve corresponds to $\mu = 0.1$.

where K_- is given by Eq. (110). The invariant profile defined by Eq. (C17) behaves as

$$f_-(\mu) \sim \frac{6^{1/4}B}{K_-} \mu^{-1/4} \sim 1.52683\dots \mu^{-1/4} \quad (\text{C19})$$

for $\mu \rightarrow +\infty$. It is plotted in Fig. 28.

The universal evolution of the radius of the BEC in scaled variables given by Eq. (C12), valid close to the critical point, is plotted in Fig. 30.

Remark: The integral of Eq. (C14) has the analytical expression

$$\begin{aligned} \int_X^{-1} \frac{dy}{\sqrt{-y^3-1}} &= \frac{2\sqrt{\pi}\Gamma(7/6)}{\Gamma(2/3)} \\ &- \frac{2}{\sqrt{-X}} {}_2F_1\left(\frac{1}{6}, \frac{1}{2}, \frac{7}{6}, -\frac{1}{X^3}\right). \end{aligned} \quad (\text{C20})$$

3. Self-similar solution with a normalization by

$$M > 1$$

Making the change of variables $y = x/\sqrt{6(M-1)}$ and introducing the scaled variables

$$T = \left(\frac{8}{3}\right)^{1/4} (M-1)^{1/4}t, \quad (\text{C21})$$

$$X(T) = \frac{x(t)}{\sqrt{6(M-1)}}, \quad X_0 = \frac{x_0}{\sqrt{6(M-1)}}, \quad (\text{C22})$$

where t , $x(t)$ and x_0 are normalized in terms of M , we can rewrite Eq. (98) as

$$\int_{X(T)}^{X_0} \frac{dy}{\sqrt{X_0 - y + X_0^3 - y^3}} = T. \quad (\text{C23})$$

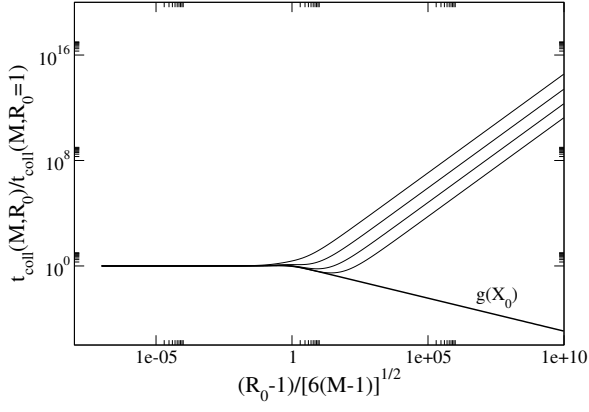


FIG. 31: Evolution of the collapse time $R_0 \mapsto t_{\text{coll}}(M, R_0)$ with $R_0 > 1$ in scaled variables. We have taken $M = 1.1, 1.01, 1.001, 1.0001$ (top to bottom). The rescaled profile converges towards the invariant profile $g(X_0)$ when $M \rightarrow 1^+$ and $R_0 \rightarrow 1^+$. It has an asymptotic logarithmic slope $-1/2$. For $R_0 \gg 1$, the self-similar solution is not valid anymore and the collapse time behaves according to Eq. (81) with a logarithmic slope $+3/2$. The two slopes, of different sign, are clearly visible on the figure.

The collapse time, corresponding to $X \rightarrow -\infty$, is given by

$$T_{\text{coll}}(X_0) = \int_{-\infty}^{X_0} \frac{dy}{\sqrt{X_0 - y + X_0^3 - y^3}}. \quad (\text{C24})$$

With the scaled variables, the collapse dynamics of the BEC close to the critical point depends on a single parameter X_0 instead of the two parameters M and R_0 . For $X_0 = 0$, we get

$$\int_{X(T)}^0 \frac{dy}{\sqrt{-y - y^3}} = T \quad (\text{C25})$$

and

$$\begin{aligned} T_{\text{coll}}(X_0 = 0) &= \int_{-\infty}^0 \frac{dy}{\sqrt{-y - y^3}} \\ &= \frac{8}{\sqrt{\pi}} \Gamma(5/4)^2 = 3.70815\dots \end{aligned} \quad (\text{C26})$$

In the general case, returning to the original variables, we obtain

$$\frac{t_{\text{coll}}(M, R_0)}{t_{\text{coll}}(M, R_0 = 1)} = g \left[\frac{R_0 - 1}{\sqrt{6(M - 1)}} \right] \quad (\text{C27})$$

where

$$g(X_0) = \frac{\int_{-\infty}^{X_0} \frac{dy}{\sqrt{X_0 - y + X_0^3 - y^3}}}{\int_{-\infty}^0 \frac{dy}{\sqrt{-y - y^3}}} \quad (\text{C28})$$

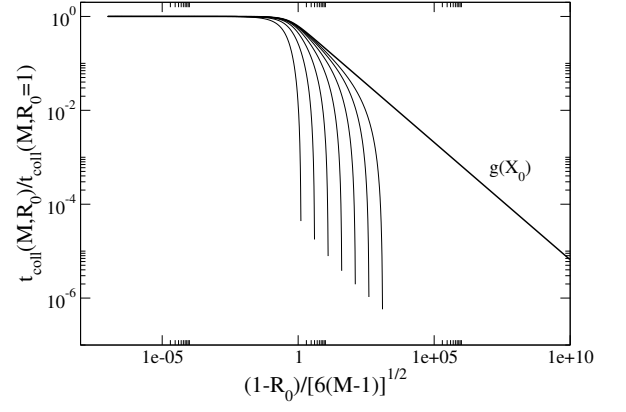


FIG. 32: Evolution of the collapse time $R_0 \mapsto t_{\text{coll}}(M, R_0)$ with $R_0 < 1$ in scaled variables. We have taken $M = 1.1, 1.01, 1.001, 1.0001, 1.00001, 1.000001, 1.0000001$ (left to right). The rescaled profile converges towards the invariant profile $g(X_0)$ when $M \rightarrow 1^+$ and $R_0 \rightarrow 1^-$. It has an asymptotic logarithmic slope $-1/2$. For $R_0 \rightarrow 0$, the self-similar solution is not valid anymore and the collapse time behaves according to Eq. (77) leading to a divergence in log-log plot.

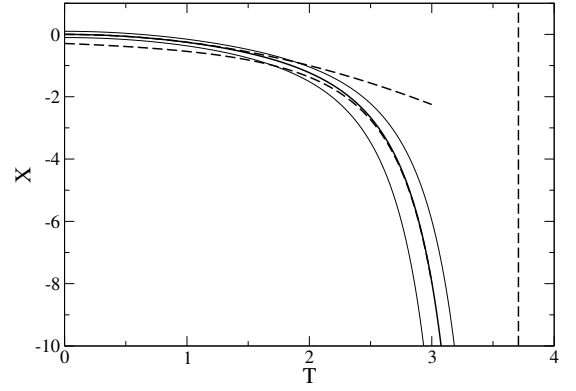


FIG. 33: Universal evolution of the scaled radius of the BEC $X(T; X_0)$ close to the critical point corresponding to a saddle-node bifurcation. The thick curve corresponds to $X_0 = 0$. According to the results of Secs. IV B and IV C, we have $X \sim -T^2/4$ for $T \rightarrow 0$ and $X \sim -4/(T_{\text{coll}} - T)^2$ for $T \rightarrow T_{\text{coll}} = 3.70815\dots$. The thin curves correspond to $X_0 = 0.1$ and $X_0 = -0.1$.

and

$$t_{\text{coll}}(M, R_0 = 1) = B(M - 1)^{-1/4}, \quad (\text{C29})$$

where B is given by Eq. (113). The invariant profile defined by Eq. (C28) behaves as

$$g(X_0) \sim \frac{K_{\pm}}{6^{1/4} B |X_0|^{1/2}} \quad (\text{C30})$$

for $X_0 \rightarrow \pm\infty$. The coefficients are 1.134408... (+) and 0.6549509... (-).

The exact collapse time given by Eq. (67) is plotted in scaled variables in Figs. 31 and 32 in order to illustrate

its convergence towards the invariant profile given by Eq. (C28) as $M \rightarrow 1^+$ and $R_0 \rightarrow 1$. The universal evolution of the radius of the BEC in scaled variables given by Eq. (C23), valid close to the critical point, is plotted in Fig. 33.

Remark: making the change of variables $y = \sinh(u)$ we also have

$$\int_{\sinh^{-1}(X(T))}^0 \frac{du}{\sqrt{-\sinh(u)}} = T \quad (\text{C31})$$

and

$$\int_{-\infty}^0 \frac{du}{\sqrt{-\sinh(u)}} = T_{\text{coll}}(X_0 = 0). \quad (\text{C32})$$

Appendix D: Particular regimes of interest

In this Appendix, we highlight particular regimes of interest considered in our paper and provide the sections where they are discussed in detail.

(i) *Self-gravity alone:* The case $E_{\text{tot}} < 0$, corresponding to the collapse of the BEC, is treated at the end of Secs. V A and V B. This solution is similar to the Mestel solution describing the gravitational collapse of a homogeneous sphere. It is also similar to a FLRW cosmological model of pressureless universe with curvature $k = +1$ exhibiting a phase of contraction (Big Crunch) after an initial phase of expansion (Big Bang). The case $E_{\text{tot}} > 0$, corresponding to the explosion of the BEC, is treated in Secs. VII C 2. This solution is similar to a FLRW cosmological model of pressureless universe with curvature $k = -1$ that is expanding. The case $E_{\text{tot}} = 0$, corresponding to a marginal case of explosion, is treated in Sec. VII C 3. This solution is similar to a FLRW cosmological model of pressureless universe without curvature ($k = 0$) known as the EdS model.

(ii) *Quantum potential alone:* The case $E_{\text{tot}} > 0$ (the only possible one), corresponding to the explosion of the BEC, is treated at the end of Sec. VIII B.

(iii) *Self-interaction alone:* The case $E_{\text{tot}} < 0$, corresponding to the collapse of the BEC, is treated at the beginning of Secs. V A and V B. The case $E_{\text{tot}} = 0$, corresponding to the marginal collapse or explosion of the BEC, is treated at the end of Sec. VIII A.

(iv) *Self-gravity and quantum potential:* The general case is treated in Sec. VIII B (the specific case of an energy $E_{\text{tot}} = 0$ is treated in Sec. VII C 3).

(v) *Self-interaction and quantum potential:* The general case is treated in Sec. VIII A.

(vi) *Self-gravity and self-interaction:* The case $E_{\text{tot}} < 0$ is treated in Sec. V.

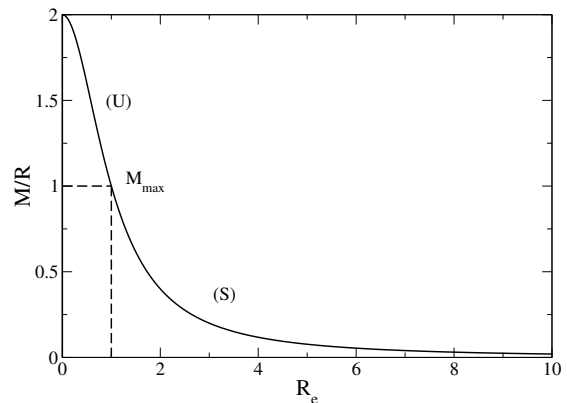


FIG. 34: Mass-radius ratio along the series of equilibria of a self-gravitating BEC with attractive self-interaction (we have used the dimensionless variables of Sec. III E).

Appendix E: Validity of the Newtonian approximation

In this Appendix, we study the validity of the Newtonian approximation used in this paper. General relativistic effects become important when the radius R of the system is of the order of the Schwarzschild radius $R_S = 2GM/c^2$. It is convenient to introduce the mass-radius ratio

$$\chi = \frac{R_S}{R} = \frac{2GM}{Rc^2}. \quad (\text{E1})$$

The Newtonian approximation is valid when $\chi \ll 1$ and general relativistic effects come into play when $\chi \sim 1$. Considering the mass-radius relation of Eq. (30), it is easy to see that the mass-radius ratio is maximum on the stable branch (S) at the point (R_*, M_{max}) . Therefore, we define

$$\chi_{\text{max}} = \frac{2GM_{\text{max}}}{R_*c^2}. \quad (\text{E2})$$

The mass-radius ratio can then be written as

$$\frac{\chi}{\chi_{\text{max}}} = \frac{M}{M_{\text{max}}} \frac{R_*}{R}. \quad (\text{E3})$$

From the mass-radius relation of Eq. (47), we get

$$\frac{\chi_e}{\chi_{\text{max}}} = \frac{2}{1 + (R_e/R_*)^2}. \quad (\text{E4})$$

This function decreases monotonically with R_e (see Fig. 34). It starts from 2 at $R_e = 0$, reaches the value 1 at $R_e = R_*$ and tends to 0 as $2/(R_e/R_*)^2$ when $R_e \rightarrow +\infty$.

Using Eqs. (35) and (36), we can write the maximum mass-radius ratio as

$$\chi_{\text{max}} = \frac{\sigma}{6\pi\zeta} \frac{2Gm}{|a_s|c^2} = \frac{\sigma}{6\pi\zeta} \frac{r_S}{|a_s|}. \quad (\text{E5})$$

In the last term, we have introduced the Schwarzschild radius $r_S = 2Gm/c^2$ of the bosons. Therefore, χ_{\max} is of the order of the ratio between the Schwarzschild radius of the bosons and their scattering length. In general, this ratio is very small ($r_S \ll |a_s|$) so that $\chi_{\max} \ll 1$, ensuring the validity of the Newtonian approximation.

To be specific, let us make a numerical application. For a standard axion particle with $m = 10^{-4} \text{ eV}/c^2$ and $a_s = -5.8 \cdot 10^{-53} \text{ m}$, we have $M_{\max} = 6.9 \times 10^{-14} M_{\odot}$ and $R_* = 1.0 \times 10^{-4} R_{\odot}$, implying $R_S = 2.93 \times 10^{-19} R_{\odot}$, $r_S = 2.65 \times 10^{-67} \text{ m}$ and $\chi_{\max} = 2.9 \times 10^{-15}$. For ultralight axions with $m = 1.93 \times 10^{-20} \text{ eV}/c^2$ and $a_s = -8.29 \times 10^{-60} \text{ fm}$, we have $M_{\max} = 4.18 \times 10^5 M_{\odot}$ and $R_* = 10.4 \text{ pc}$, implying $R_S = 4.00 \times 10^{-8} \text{ pc}$, $r_S = 5.11 \times 10^{-83} \text{ m}$ and $\chi_{\max} = 3.85 \times 10^{-9}$. These two systems, which correspond respectively to axion stars and axionic dark matter halos, can be treated by Newtonian gravity since $\chi_{\max} \ll 1$.

When $M > M_{\max}$, the system collapses and ultimately forms a black hole. Since $R(t) \rightarrow 0$ as $t \rightarrow t_{\text{coll}}$, there exists a time t_{GR} at which general relativity has to be taken into account. We define it such that $R(t_{\text{GR}}) = R_S$ or, equivalently, $\chi(t_{\text{GR}}) = 1$. Using Eq. (E3), it corresponds to $[R(t_{\text{GR}})/R_*]/[M/M_{\max}] = \chi_{\max}$. When t_{GR} is close to t_{coll} , we can use the asymptotic formula

of Eq. (73). This gives

$$\Delta t = t_{\text{coll}} - t_{\text{GR}} = \left(\frac{6}{25}\right)^{1/2} \chi_{\max}^{5/2} \left(\frac{M}{M_{\max}}\right)^2 t_D. \quad (\text{E6})$$

For standard axions with $m = 10^{-4} \text{ eV}/c^2$ and $a_s = -5.8 \cdot 10^{-53} \text{ m}$, assuming $M = 2M_{\max} = 1.4 \times 10^{-13} M_{\odot}$ and $R_0 = R_* = 1.0 \times 10^{-4} R_{\odot}$, we find $t_D = 3.4 \text{ hrs}$, $t_{\text{coll}} = 2.3 \text{ hrs}$, and $\Delta t = 1.09 \times 10^{-32} \text{ s}$. For ultralight axions with $m = 1.93 \times 10^{-20} \text{ eV}/c^2$ and $a_s = -8.29 \times 10^{-60} \text{ fm}$, assuming $M = 2M_{\max} = 8.36 \times 10^5 M_{\odot}$ and $R_0 = R_* = 10.4 \text{ pc}$, we find $t_D = 1.49 \text{ Myrs}$, $t_{\text{coll}} = 1.01 \text{ Myrs}$ and $\Delta t = 8.47 \times 10^{-8} \text{ s}$. In each case, general relativistic effects become important only extraordinarily close to the collapse time.

Remark: For consistency, we have used the result of Eq. (73) based on the Gaussian ansatz. However, we have mentioned at the end of Sec IV C that this result may not be accurate. Using the exact result of [102] does not change our conclusion that general relativistic effects become important only extraordinarily close to the collapse time. This is intrinsically due to the fact that $R \rightarrow 0$ as $t \rightarrow t_{\text{coll}}$ with an infinite slope.

-
- [1] M.R. Baldeschi, G.B. Gelmini, R. Ruffini, Phys. Lett. B **122**, 221 (1983)
- [2] M.Yu. Khlopov, B.A. Malomed, Ya.B. Zeldovich, Mon. Not. R. astr. Soc. **215**, 575 (1985)
- [3] M. Membrado, A.F. Pacheco, J. Sanudo, Phys. Rev. A **39**, 4207 (1989)
- [4] S.J. Sin, Phys. Rev. D **50**, 3650 (1994)
- [5] S.U. Ji, S.J. Sin, Phys. Rev. D **50**, 3655 (1994)
- [6] J.W. Lee, I. Koh, Phys. Rev. D **53**, 2236 (1996)
- [7] F.E. Schunck, [astro-ph/9802258]
- [8] T. Matos, F.S. Guzmán, F. Astron. Nachr. **320**, 97 (1999)
- [9] F.S. Guzmán, T. Matos, Class. Quantum Grav. **17**, L9 (2000)
- [10] W. Hu, R. Barkana, A. Gruzinov, Phys. Rev. Lett. **85**, 1158 (2000)
- [11] P.J.E. Peebles, Astrophys. J. **534**, L127 (2000)
- [12] J. Goodman, New Astronomy **5**, 103 (2000)
- [13] T. Matos, L.A. Ureña-López, Phys. Rev. D **63**, 063506 (2001)
- [14] A. Arbey, J. Lesgourgues, P. Salati, Phys. Rev. D **64**, 123528 (2001)
- [15] M.P. Silverman, R.L. Mallett, Class. Quantum Grav. **18**, L103 (2001)
- [16] M. Alcubierre, F.S. Guzmán, T. Matos, D. Núñez, L.A. Ureña-López, P. Wiederhold, Class. Quantum. Grav. **19**, 5017 (2002)
- [17] M.P. Silverman, R.L. Mallett, Gen. Rel. Grav. **34**, 633 (2002)
- [18] J. Lesgourgues, A. Arbey, P. Salati, New Astron. Rev. **46**, 791 (2002)
- [19] A. Arbey, J. Lesgourgues, P. Salati, Phys. Rev. D **68**, 023511 (2003)
- [20] C.G. Böhrer, T. Harko, J. Cosmol. Astropart. Phys. **06**, 025 (2007)
- [21] A. Bernal, T. Matos, D. Núñez, Rev. Mex. Astron. Astrofis. **44**, 149 (2008)
- [22] P. Sikivie, Q. Yang, Phys. Rev. Lett. **103**, 111301 (2009)
- [23] T. Matos, A. Vázquez-González, J. Magaña, Mon. Not. R. Astron. Soc. **393**, 1359 (2009)
- [24] J.W. Lee, Phys. Lett. B **681**, 118 (2009)
- [25] T.P. Woo, T. Chiueh, Astrophys. J. **697**, 850 (2009)
- [26] J.W. Lee, S. Lim, J. Cosmol. Astropart. Phys. **01**, 007 (2010)
- [27] P.H. Chavanis, Phys. Rev. D **84**, 043531 (2011)
- [28] P.H. Chavanis, L. Delfini, Phys. Rev. D **84**, 043532 (2011)
- [29] P.H. Chavanis, Phys. Rev. D **84**, 063518 (2011)
- [30] F. Briscece, Phys. Lett. B **696**, 315 (2011)
- [31] T. Harko, Mon. Not. R. Astron. Soc. **413**, 3095 (2011)
- [32] T. Harko, J. Cosmol. Astropart. Phys. **05**, 022 (2011)
- [33] A. Suárez, T. Matos, Mon. Not. R. Astron. Soc. **416**, 87 (2011)
- [34] P.H. Chavanis, Astron. Astrophys. **537**, A127 (2012)
- [35] H. Velten, E. Wamba, Phys. Lett. B **709**, 1 (2012)
- [36] M.O.C. Pires, J.C.C. de Souza, J. Cosmol. Astropart. Phys. **11** (2012) 024
- [37] C.-G. Park, J.-C. Hwang, H. Noh, Phys. Rev. D **86**, 083535 (2012)
- [38] V.H. Robles, T. Matos, Monthly Not. Roy. Astron. Soc. **422**, 282 (2012)
- [39] T. Rindler-Daller, P. R. Shapiro, Monthly Not. Roy. Astron. Soc. **422**, 135 (2012)
- [40] V. Lora, J. Magaña, A. Bernal, F.J. Sánchez-Salcedo,

- E.K. Grebel, *J. Cosmol. Astropart. Phys.* **02**, 011 (2012)
- [41] J. Magaña, T. Matos, A. Suárez, F. J. Sánchez-Salcedo, *JCAP* **10**, 003 (2012)
- [42] G. Manfredi, P.A. Hervieux, F. Haas, *Class. Quantum Grav.* **30**, 075006 (2013)
- [43] A.X. González-Morales, A. Diez-Tejedor, L.A. Ureña-López, O. Valenzuela, *Phys. Rev. D* **87**, 021301(R) (2013)
- [44] F.S. Guzmán, F.D. Lora-Clavijo, J.J. González-Avilés, F.J. Rivera-Paleo, *J. Cosmol. Astropart. Phys.* **09** (2013) 034
- [45] H.Y. Schive, T. Chiueh, T. Broadhurst, *Nature Physics* **10**, 496 (2014)
- [46] H.Y. Schive *et al.*, *Phys. Rev. Lett.* **113**, 261302 (2014)
- [47] B. Li, T. Rindler-Daller, P.R. Shapiro, *Phys. Rev. D* **89**, 083536 (2014)
- [48] D. Bettoni, M. Colombo, S. Liberati, *JCAP* **02**, 004 (2014)
- [49] V. Lora, J. Magaña, *JCAP* **09**, 011 (2014)
- [50] P.H. Chavanis, *Eur. Phys. J. Plus* **130**, 180 (2015)
- [51] E.J.M. Madarassy, V.T. Toth, *Phys. Rev. D* **91**, 044041 (2015)
- [52] A. Suárez, P.H. Chavanis, *Phys. Rev. D* **92**, 023510 (2015)
- [53] A. Suárez, P.H. Chavanis, *J. Phys.: Conf. Series* **654**, 012088 (2015)
- [54] P.H. Chavanis, *Phys. Rev. D* **92**, 103004 (2015)
- [55] A.H. Guth, M.P. Hertzberg, C. Prescod-Weinstein, *Phys. Rev. D* **92**, 103513 (2015)
- [56] J.C.C. de Souza, M. Ujevic, *Gen. Relat. Grav.* **47**, 100 (2015)
- [57] R.C. de Freitas, H. Velten, *Eur. Phys. J. C* **75**, 597 (2015)
- [58] J. Alexandre, *Phys. Rev. D* **92**, 123524 (2015)
- [59] K. Schroyen, M. List, C. Lämmerzahl, *Phys. Rev. D* **92**, 124008 (2015)
- [60] J. Eby, C. Kouvaris, N.G. Nielsen, L.C.R. Wijewardhana, *JHEP* **02**, 028 (2016)
- [61] J.A.R. Cembranos, A.L. Maroto, S.J. Núñez Jareño, *JHEP* **03**, 013 (2016)
- [62] E. Braaten, A. Mohapatra, H. Zhang, [arXiv:1502.00108]
- [63] S. Davidson, T. Schwetz, [arXiv:1603.04249]
- [64] J. Fan, [arXiv:1603.06580]
- [65] E. Calabrese, D.N. Spergel [arXiv:1603.07321]
- [66] A. Suárez, V.H. Robles, T. Matos, *Astrophys. Space Sci. Proc.* **38**, 107 (2014)
- [67] T. Rindler-Daller, P.R. Shapiro, *Astrophys. Space Sci. Proc.* **38**, 163 (2014)
- [68] P.H. Chavanis, *Self-gravitating Bose-Einstein condensates*, in *Quantum Aspects of Black Holes*, edited by X. Calmet (Springer, 2015)
- [69] E. Madelung, *Zeit. F. Phys.* **40**, 322 (1927)
- [70] D.J. Kaup, *Phys. Rev.* **172**, 1331 (1968)
- [71] R. Ruffini, S. Bonazzola, *Phys. Rev.* **187**, 1767 (1969)
- [72] M. Colpi, S.L. Shapiro, I. Wasserman, *Phys. Rev. Lett.* **57**, 2485 (1986)
- [73] P.H. Chavanis, T. Harko, *Phys. Rev. D* **86**, 064011 (2012)
- [74] J. M. Lattimer and M. Prakash, in *From Nuclei to Stars*, Ed: S. Lee (Singapore, World Scientific, 2011), [arXiv:1012.3208]
- [75] P. B. Demorest, T. Pennucci, S. M. Ransom, M. S. E. Roberts and J. W. T. Hessels, *Nature* **467**, 1081 (2010)
- [76] O. Barziv, L. Karper, M. H. van Kerkwijk, J. H. Telging, and J. van Paradijs, *Astron. Astrophys.* **377**, 925 (2001)
- [77] H. Quaintrell, A. J. Norton, T. D. C. Ash, P. Roche, B. Willems, T. R. Bedding, I. K. Baldry, and R. P. Fender, *Astron. Astrophys.* **401**, 303 (2003)
- [78] M. H. van Kerkwijk, R. Breton, and S. R. Kulkarni, *Astrophys. J.* **728**, 95 (2011)
- [79] J. Antoniadis *et al.*, *Science* **340**, 6131 (2013)
- [80] J.R. Oppenheimer, G.M. Volkoff, *Phys. Rev.* **55**, 374 (1939)
- [81] J.E. Kim, G. Carosi, *Rev. Mod. Phys.* **82**, 557 (2010)
- [82] D. Marsh, [arXiv:1510.07633]
- [83] R.D. Peccei, H.R. Quinn, *Phys. Rev. Lett.* **38**, 1440 (1977)
- [84] A. Arvanitaki, S. Dimopoulos, S. Dubovsky, N. Kaloper, J. March-Russell, *Phys. Rev. D* **81**, 123530 (2010)
- [85] P. Sikivie, Q. Yang, *Phys. Rev. Lett.* **103**, 111301 (2009)
- [86] O. Erken, P. Sikivie, H. Tam, Q. Yang, *Phys. Rev. D* **85**, 063520 (2012)
- [87] P.H. Chavanis, M. Lemou, F. Méhats, *Phys. Rev. D* **92**, 123527 (2015)
- [88] J.F. Navarro, C.S. Frenk, S.D.M. White, *Astrophys. J.* **462**, 563 (1996)
- [89] E. Seidel, W.M. Suen, *Phys. Rev. Lett.* **72**, 2516 (1994)
- [90] P.H. Chavanis, in preparation
- [91] E.P. Gross, *Ann. of Phys.* **4**, 57 (1958); *Nuovo Cimento* **20**, 454 (1961); *J. Math. Phys.* **4**, 195 (1963)
- [92] L.P. Pitaevskii, *Sov. Phys. JETP* **9**, 830 (1959); *ibid* **13**, 451 (1961)
- [93] N. Bogoliubov, *J. Phys.* **11**, 23 (1947)
- [94] F. Dalfovo, S. Giorgini, L.P. Pitaevskii, S. Stringari, *Rev. Mod. Phys.* **71**, 463 (1999)
- [95] S. Chandrasekhar, *An Introduction to the Study of Stellar Structure* (Dover, 1958)
- [96] D.D. Holm, J.E. Marsden, T. Ratiu, A. Weinstein, *Phys. Rep.* **123**, 1 (1985)
- [97] S. Weinberg, *Gravitation and Cosmology* (John Wiley, 2002)
- [98] P.H. Chavanis, *Eur. Phys. J. Plus* **129**, 38 (2014)
- [99] H. Poincaré, *Acta Math.* **7**, 259 (1885)
- [100] J. Katz, *Mon. Not. R. Astron. Soc.* **183**, 765 (1978)
- [101] P.H. Chavanis, *Int. J. Mod. Phys. B* **20**, 3113 (2006)
- [102] C. Sulem, P.L. Sulem, *The Nonlinear Schrödinger Equation* (Springer, 1999)
- [103] L. Mestel, *Q. Jl R. Astr. Soc.* **6**, 161 (1965)
- [104] Y. Pomeau, M. Le Berre, P.H. Chavanis, B. Denet, *Eur. Phys. J. E* **37**, 26 (2014)
- [105] E.A. Donley, N.R. Claussen, S.L. Cornish, J.L. Roberts, E.A. Cornell, C.E. Wieman, *Nature* **412**, 295 (2001)